

A search for tight hierarchical triple systems amongst the eclipsing binaries in the CoRoT fields

T. Hajdu,^{1,2*} T. Borkovits,^{3,4} E. Forgács-Dajka,¹ J. Sztakovics,^{1,2} G. Marschalkó,^{2,3}
J. M. Benkő,⁴ P. Klagyivik,⁴ and M. J. Sallai¹

¹*Eötvös University, Department of Astronomy, H-1118 Pázmány Péter stny. 1/A, Budapest, Hungary*

²*Wigner Research Centre for Physics of HAS, PO Box 49, H-1525, Budapest, Hungary*

³*Baja Astronomical Observatory of Szeged University, H-6500 Baja, Szegedi út, Kt. 766, Hungary*

⁴*Konkoly Observatory, Research Centre for Astronomy and Earth Sciences, Hungarian Academy of Sciences, H-1121 Budapest, Konkoly Thege Miklós út 15-17, Hungary*

Accepted XXX. Received YYY; in original form ZZZ

ABSTRACT

We report a comprehensive search for hierarchical triple stellar system candidates amongst eclipsing binaries (EB) observed by the CoRoT spacecraft. We calculate and check eclipse timing variation (ETV) diagrams for almost 1500 EBs in an automated manner. We identify five relatively short-period Algol systems for which our combined light curve and complex ETV analyses (including both the light-travel time effect and short-term dynamical third-body perturbations) resulted in consistent third-body solutions. The computed periods of the outer bodies are between 82 and 272 days, (with an alternative solution of 831 days for one of the targets). We find that the inner and outer orbits are near coplanar in all but one case. The dynamical masses of the outer subsystems determined from the ETV analyses are consistent with both the results of our light curve analyses and the spectroscopical information available in the literature. One of our candidate systems exhibits outer eclipsing events as well, the locations of which are in good agreement with the ETV solution. We also report another certain triply eclipsing triple system which, however, is lacking a reliable ETV solution due to the very short time range of the data, and four new blended systems (composite light curves of 2 eclipsing binaries each), where we cannot decide whether the components are gravitationally binded or not. Amongst these blended systems we identify the longest period and highest eccentricity eclipsing binary in the entire CoRoT sample.

Key words: methods: analytical – binaries: close – binaries: eclipsing

1 INTRODUCTION

Multiplicity is a common feature amongst binary star systems. For example, according to an investigation of Tokovinin et al. (2006) almost two thirds of their surveyed 165 solar-type spectroscopic binary systems have at least one more stellar companion. Furthermore, in the same sample, amongst the shortest period binaries ($P \leq 2^d$) this ratio practically reaches 100%. These findings are in good agreement with the recently most commonly accepted formation theory of the closest binary systems (typically with periods of a few days), the so called Kozai Cycles with Tidal Friction (KCTF) mechanism, which first was proposed by Kiseleva et al. (1998) and later was quantitatively investigated in de-

tails by e.g., Fabrycky & Tremaine (2007); Naoz & Fabrycky (2014). Multiplicity, however, may have fundamental influence on binary star evolution (and, of course, directly or indirectly on the stellar evolution of binary members) not only in the formation period of a binary system, but at every stage of its evolution from the birth to the death of the binary members. Some examples are the hypothesised importance of multiplicity in the formation of blue stragglers (Perets & Fabrycky 2009; Naoz & Fabrycky 2014), and different kinds of binaries formed by degenerate components (Shappee & Thompson 2013; Naoz et al. 2016). Furthermore, Tauris & van den Heuvel (2014) amongst others have shown that the presence of a third stellar component may prevent a close binary system from disintegration even when one of its components undergoes a supernova explosion. Therefore, the identification of third (or even more) additional stellar companions to binary star systems has great astrophysical

* E-mail: t.hajdu@astro.elte.hu

importance both from a general theoretical perspective (as probing the current theories) and on the other hand to understand the evolution of any given, individual system.

In the case of eclipsing binaries (EB) one long-lasting, traditionally used method for the identification of third, more distant companions is based on the detection and analysis of the eclipse timing variations (ETV) of the binary star which occur due to the light-travel time effect (LTTE) as the EBs distance to the observer periodically varies revolving on its orbit around the common centre of mass of the triple (or multiple) system.

According to our knowledge, [Chandler \(1888\)](#) was the first who mentioned LTTE as a possible origin of the observed ETVs of Algol. After the preliminary analytical works of [Woltjer \(1922\)](#), the widely used mathematical description of an LTTE forced ETV was given by [Irwin \(1952, 1959\)](#) who also gave a graphical fitting procedure for determining the elements of the light-time orbit from the ETVs that had been traditionally investigated by the use of eclipse timing diagrams, which in the century-long history of the variable star research traditionally was called as $O-C$ (observed minus calculated) diagram (see e.g. [Sterken 2005](#), for a short review on the advantages and obstacles of the application of $O-C$ diagrams in the analysis of period variations of different kinds of variable stars).

There are, however, various other mechanisms capable to produce ETVs in EBs, some of them may even strongly mimic LTTE-like behaviour. Therefore, certain detection of third components in such a manner is far from being an easy matter. In this regard [Frieboes-Conde & Herczeg \(1973\)](#) listed four criteria that an ETV curve should fulfil for an LTTE solution which can be taken seriously. These criteria can be summarized as follows. (1) The shape of the ETV curve must follow the analytical form of an LTTE solution. (2) The ETVs of the primary and secondary minima must be consistent in both phase and amplitude with each other. (3) The estimated mass or lower limit to the mass of the third component, derived from the amplitude of the LTTE solution must be in accord with photometric measurements or limits on third light in the system. (4) Variation of the systemic radial velocity (if it is available) should be in accord with the LTTE solution. Recently this list was complemented with two subsequent criteria by [Borkovits et al. \(2016\)](#), as follows. (5) The times of the maxima of the ellipsoidal variations (if they are detectable with sufficient accuracy), at least in EBs that have circular orbits, should be in accord both in phase and amplitude with the ETVs. Furthermore, for triples exhibiting outer eclipses, an additional natural criterion for identifying the outer eclipsing body with the source of the observed LTTE is that (6) the LTTE should exhibit the same period as the extra eclipses, and these latter should occur around the inferior and/or superior conjunction points of the LTTE-orbit.¹

Before the era of small, but ultraprecise photometric

space telescopes (e.g. as CoRoT and *Kepler*) the vast majority of the known third companions (or, more strictly, candidates) had orbital periods of several years or, even decades, and only a very limited number of hierarchical triple systems with outer periods less than a year were known (see e.g. [Tokovinin 2004](#)). As dynamical stability criteria (see e.g. [Mardling & Aarseth 2001](#)) would allow the presence of 1-2-month-long outer period stellar companion to a typical eclipsing binary with period from a few hours to few days, it was not clear whether the small known number of such systems was a consequence of some selection effects, or of yet-unknown evolutionary origin(s) (see e.g. [Tokovinin 2014](#)). In this regard the four-year-long almost continuous measurements of *Kepler* spacecraft ([Borucki et al. 2010](#)) resulted in a significant improvement, allowing to explore regions of the parameter space previously out of the reach of ground-based ETV studies due to the small LTTE amplitude involved, like triple stellar systems in the shortest theoretically possible outer period regime. Systematic analyses of the ETVs of more than 2700 EBs (and ellipsoidal variables), observed continuously during the prime *Kepler* mission have led to the discovery of more than 200 hierarchical triple system candidates ([Rappaport et al. 2013](#); [Conroy et al. 2014](#); [Borkovits et al. 2015](#); [Gies et al. 2015](#); [Borkovits et al. 2016](#); [Kirk et al. 2016](#)). Considering e.g. the survey of [Borkovits et al. \(2016\)](#), more than a hundred of the 222 triple system candidates investigated by them have outer periods less than 1000 days.

The observing strategy, i.e. the short, four-five month-long observing sessions of the complemented and contemporary mission of the European CoRoT spacecraft ([Auvergne et al. 2009](#)), however, unfortunately, was less favourable from the point of view of searching for additional, distant companions around EBs by the use of ETV analysis. This particularly holds when we restrict ourselves to the most certain detections which, according to the criteria of [Conroy et al. \(2014\)](#) and similarly, of [Borkovits et al. \(2016\)](#) require at least two fully covered orbital periods of the outer orbit to be observed. On the other hand, in a less restrictive sense the 100-150-day long CoRoT ETV data series may allow us to identify some of the tightest triple star candidates. For example, the work of [Borkovits et al. \(2016\)](#) mentioned above reported 13 triples (i.e. approximately 0.5% of the total number of the *Kepler* EBs) with outer period less than 150 days. The characteristic shape of the ETVs of the majority of these tightest triple systems would allow us to identify them as probable triple system candidates even from the short ETV sections available from CoRoT observations.

A further glance at the results of [Borkovits et al. \(2016\)](#) reveals that in the ETVs of these tight systems the dynamical, hierarchical third-body perturbations play a dominant role, or are at least as important in magnitude as the classical LTTE, therefore their contribution should also be taken into account. This latter, dynamical ETV contribution was analytically described in a series of papers by [Borkovits et al. \(2003, 2011, 2015\)](#). (Some preliminary works on this field had also been carried out by [Soderhjelm 1975](#) and [Mayer 1990](#).)

In this paper we are searching for hierarchical triple star candidates amongst the EBs observed by the CoRoT spacecraft, primarily with the analysis of their ETVs. For the analysis we use publicly available CoRoT photometric data. In Section 2 we outline the steps of our investigation, starting

¹ Thanks to some remarks of the referee of the present paper we realized that this last criterium was set erroneously in [Borkovits et al. \(2016\)](#), where, originally, it was stated that the outer eclipses “should occur around the extrema of the LTTE”. This latter statement is strictly valid only in the case of a circular outer orbit or an orbit seen from the direction of its major axis.

with the methods used for data acquisition and automatic ETV curve generation, then continuing with the system selection procedures and, finally, closing with a short description of some details of the applied ETV and the auxiliary light curve analyses as well.

The results of the detailed analysis of the ETV and light curves of the five newly identified tight hierarchical triple candidates as well as some other interesting by-products of our research, are discussed in Sections 3 and 4.

Finally, a short summary is given in Section 5.

2 BASIC STEPS OF THE ANALYSIS

2.1 Data acquisition and preparation

The space mission CoRoT performed wide-field stellar photometry at ultra-high precision (Rouan et al. 1998; Baglin et al. 2006). The mission took 6 years from the end of 2006 to the November of 2012. During an observation, up to 12 000 stars were monitored simultaneously and continuously over 150 days of observation. All observations of CoRoT spacecraft, the so-called LEGACY data (version 4, see Chaintreuil et al. 2016) are publicly available now, e.g. through the VizieR archive service².

We downloaded all the corrected (LCC, see Chaintreuil et al. 2016, Sect. 1.2) light curves of the CoRoT Bright and Faint Star Catalogs. Then we performed a visual inspection of all the over 177 700 light curves individually, and identified about 1500 EBs (including binaries with ellipsoidal variations, but without real eclipses, too). This number is nearly the same as the one reported in Baudin et al. (2016). Unfortunately, these authors do not give the complete list of these EBs, therefore we were unable to cross-check our findings with theirs. We made comparison, however, with the so-called “Unofficial CoRoT Eclipsing Binary Catalog” of Jonathan Devor³, which contains also 1479 items. Surprisingly, there is a remarkable ($\approx 40\%$) amount of mismatch between our findings and this latter catalog. In our opinion, several very short period ($P \lesssim 0^d.15$), low amplitude ($\lesssim 1\%$ in normalized flux) light curves listed in Devor’s catalog should belong to pulsating stars rather than eclipsing or ellipsoidal variables and, therefore, we do not count them amongst the CoRoT EBs. On the other hand, a significant amount of certain CoRoT EBs are not included into this unofficial catalog, the triply eclipsing CoRoT 104079133 (i.e. one of the five EBs which we study in this paper in details) being a notable example.

We then prepared the light curves of these EBs for the forthcoming analysis in an iterative and automatic manner, using our own GPU-based code, written in CUDA language.

As a first step, the code determines preliminary eclipsing periods for each EB using the Lomb-Scargle periodogram method. Then, using these periods, it creates folded, binned, averaged light curves for each EBs in the following manner. The light curves are binned into 500-1000 equally spaced phase-cells, according to the orbital phases of each measured point. Then the average fluxes are calculated cell by cell, and associated to the phase of the cell midpoints. In the

next step the code identifies the locations (phase-domains) of the eclipses (primary and secondary) in the folded light curves, and then calculates template minima, fitting sixth-order polynomials on the previously identified phase ranges.

In the next part of the analysis the code scans the original light curves of each EB, identifies all the individual primary and secondary eclipses, and applies the appropriate template minimum for the determination of the individual mid-minimum moments. For this purpose the code fits a three-parameter model to the data with the Levenberg–Marquardt method. The fitted template curve is the following:

$$f'(x) = a_0 + a_1 \cdot f(x - a_2) \quad (1)$$

where $f(x)$ is the previously determined polynomial template function, and the most important parameter is a_2 , which gives the phase-lag between the template and the current eclipse (see Borkovits et al. 2015, Sect. 4, for further details).

In the last step the code calculates ETV diagrams using the preliminary period obtained in the very first step, and determines the average slope of each ETV curve with linear regression. The period is then corrected with this average slope (and the epoch, i.e. the moment of the zero phase is corrected, too), and the whole procedure is reiterated until convergence of the period. We found that two iteration steps were enough for all light curves.

Extra care was required for some of the light curves, due to the presence of extra-eclipsing events. The data points affected by these extra events were excluded from both the light curve folding and the ETV forming procedures.

2.2 System selection

For further analysis we selected (by visual inspection) systems having sine-like variations or at least significant curvature(s) in their ETV curve(s). We dropped out, however, some short period (most probably overcontact) binaries where the primary and secondary ETVs exhibited quasi-sinusoidal variations in opposite phase to each other, which might be the product of light curve distortions originating from stellar spot rotation (Tran et al. 2013; Balaji et al. 2015). We investigated the ETVs of EBs showing clearly visible extra eclipsing events with extra care. Finally, we found five EBs in the investigated CoRoT sample for which we were able to obtain preliminary ETV solutions. Then in the last step we carried out a more complex study of these EBs, including light curve analyses, too.

2.3 Analysis of the folded light curves

The supplementary light curve analyses of the selected systems were carried as follows. Rather than conducting a more sophisticated investigation, our primary aim was to obtain the values of those parameters from the light curve that provide significant auxiliary information to the ETV analysis. These parameters are the eccentricity (e_1) and argument of periastron (ω_1) of the eclipsing pairs, and the amount of the third light (l_3) in the light curve. The photometrically obtained values of e_1 and ω_1 can be used directly for the ETV analysis (see below), while the presence (or absence) of an extra light source (and its light ratio) may be a good additional indicator of the reliability of our third-body solutions.

² <http://vizier.u-strasbg.fr/viz-bin/VizieR?-source=B/corot>

³ http://www.astro.tau.ac.il/~jdevor/CoRoT_catalog/catalog.html

For this study we used the folded and binned, averaged CoRoT light curves. The analysis of these light curves was carried out with an MCMC-based parameter search which was recently incorporated into the newest version of our own LIGHTCURVEFACTORY light curve synthesis program (Borkovits et al. 2013, 2014). We used an own implementation of the generic Metropolis-Hastings algorithm, and uniform priors. For the sake of a quick convergence we used in general a special set of nine adjusted parameters. These were as follows: (i) length of the primary eclipse (Δt); (ii) ratio of the stellar radii (R_B/R_A)⁴; (iii) mass ratio ($q_1 = m_B/m_A$); (iv) temperature ratio ($T_{\text{eff},B}/T_{\text{eff},A}$); (v) eccentricity (e_1); (vi) mid-phase of the secondary eclipse (ϕ_{II}); (vii) mid-time of the primary eclipse; (viii) inclination (i_1); (ix) third light (I_3)⁵. Then the additional system parameters like the fractional radii of the two stars ($r_{A,B} = R_{A,B}/a_1$) and the remaining orbital parameters (argument of periastron – ω_1 and periastron passage time – τ_1 , or its some equivalents) were calculated by the use of the relations given in Rappaport et al. (2017, Eq. 6–10). The advantage of this set of parameters is that three of them (i, vi and vii) are direct observables and therefore their initial values can be determined very easily from the folded light curve. According to our experiences, if the initial values of these three parameters are set properly, then our Markov Chains converged quickly for any arbitrary (but physically realistic) initial values of the other parameters. Regarding the mass ratio (q_1), however, some caution has to be taken. For detached EBs with almost spherical stellar components, the mass ratio has only minor influence on the light curve, therefore pure light curve analysis can derive its actual value only with a large uncertainty. This is especially true when other complicating effects (like chromospheric activity, pulsation, etc.) distort the light curves with magnitudes similar to (or greater than) the mass ratio dependent effects. This was exactly the situation for CoRoT 110830711. Therefore in this case we used some astrophysical constraints for q_1 , as discussed in Sect. 3.1.

Regarding other, higher order effects influencing a light curve solution, ellipsoidal variation, Doppler-boosting and reflection/irradiation effects were also taken into account in our analysis. Limb darkening was considered according to the logarithmic law (Klinglesmith & Sobieski 1970). The corresponding coefficients were computed internally by the use of the “in-house tables” of the Phoebe software⁶ (Prša & Zwitter 2005). In case of CoRoT 102698865, however, the use of these precomputed coefficients resulted in systematically biased residuals during the eclipses with a magnitude of about 3-4000 ppm, which diminished remarkably when the adjustment of these parameters was switched on.

The results of our analysis on the selected five EBs will be discussed in Sect. 3. Here we only briefly mention that

three of the five EBs were found to be dominated by the flux(es) of extra source(s). As a consequence, we may assume that for these three systems the spectroscopic information e. g. temperature, spectral type given either in the ExoDat Information System⁷ (Deleuil et al. 2009), or in Sarro et al. (2013) may refer to the extra source(s) and therefore, unfortunately, we cannot use them with full confidence to convert the direct outputs of the light curve analysis, which are dimensionless, relative quantities (e. g. temperature and mass ratios, and the dimensions of the stars relative to the semi-major axis) to physical units. There are, however, two possibilities for getting some information, or at least reasonable estimations, for the real nature of the binary components.

First, the combination of the relative stellar radii and the mass ratio offer an indirect possibility to infer at least a probable luminosity class for the binary components via a reliable estimation of the local surface gravity (g). In order to show this, we approximate the local surface gravity of (let’s say), the primary component as:

$$g_A = \frac{Gm_A}{r_A^2 a_1^2}, \quad (2)$$

which, by the use of Kepler’s third law can be written as

$$\begin{aligned} g_A &= r_A^{-2} \left(\frac{2\pi}{P_1} \right)^{4/3} \frac{(Gm_A)^{1/3}}{(1+q_1)^{2/3}} \\ &= g_A^* m_A^{1/3}, \end{aligned} \quad (3)$$

where g_A^* can be calculated directly from the light curve solution. (For the secondary component q_1 should be replaced with q_1^{-1} .) Expressing g in its usual logarithmic form (and using the usual astrophysical units)

$$\log g_A = \log g_A^* + \frac{1}{3} \log m_A, \quad (4)$$

it can be seen that the mass-dependent, unknown last term gives only a minor contribution to the sum for a wide range of the physically reasonable stellar masses (cf. Southworth et al. 2004). Therefore $\log g_A^*$ can be used as a good estimate of $\log g_A$ and thus of the probable luminosity class of the given star.⁸

Second, as it will be discussed in the next subsection, by combining the outputs of the light curve analysis with the results of a joint LTTE+dynamical ETV analysis, we can infer the masses of the EB components in a dynamical way.

⁷ <http://cesam.oamp.fr/exodat/>

⁸ On the other hand, however, one should again keep in mind that, as discussed above, the photometric mass ratio q_1 is a weakly determined quantity for our detached EBs. This results in an uncertainty in $\log g^*$ and, therefore, in the estimated local surface gravity. From Eq. (3) one can see that for the more massive component (i.e. for which $q \leq 1$) this uncertainty has an upper limit of $\Delta \log g_{(q \leq 1)}^* \leq \frac{2}{3} \log 2 \approx 0.2$. For the less massive component there is no such upper limit. Conversely, for extreme mass ratios, the uncertainty, in theory, may tend to infinity. In practice it can be used an additional indicator of inappropriate light curve solutions with unphysical mass-ratios.

⁴ In order to avoid confusion we use numerical indices, (i.e. 1 and 2) only for the quantities referring to the inner and outer orbits, while the parameters associated with the stellar components are indexed with capitals, with A, B and C marking the primary and secondary components of the inner (eclipsing) binary, and the the third, more distant component, respectively.

⁵ We emphasize again that the light curve analyses were carried out on phase-folded light curves. Thus, the orbital period (P_1) was not an adjustable parameter.

⁶ <http://phoebe-project.org/1.0>

2.4 Overview of the ETV analysis

The ETV analysis of each system was carried out with the newest version of the OMNIFIT code of T. Borkovits. This version differs from the previous ones only by the inclusion of an MCMC-based parameter search. The theoretical base and the applied analytical formalism of the analysis remained unchanged, however, and was described in detail in Borkovits et al. (2015, 2016). Therefore here we give only a brief summary.

We define ETV as the time difference of the observed and calculated mid-minima times of each individual eclipses:

$$\Delta = T(E) - T_0 - P_s E, \quad (5)$$

where $T(E)$ stands for the observed mid-minimum time of the E th eclipse (cycle number E is integer for primary and half-integer for secondary eclipses, respectively), T_0 indicates the reference epoch, i.e. the observed mid-eclipse time of the ‘zeroth’ event, and P_s is the constant sidereal (eclipse) period. The ETV is then basically modelled in the following form:

$$\Delta = c_0 + c_1 E + [\Delta_{\text{LTTE}} + \Delta_{\text{dyn}} + \Delta_{\text{apse}}]_0^E, \quad (6)$$

where $c_{0,1}$ give corrections to the reference epoch and the eclipse period, respectively (independent on their origins), while Δ_{LTTE} , Δ_{dyn} , and Δ_{apse} refer to the contributions of LTTE, short-period dynamical third-body perturbations (i.e. those with periods equal to, or related to the orbital period P_2 of the third, outer component), and apsidal motion effect to the ETVs, respectively.

The LTTE contribution takes the following form (Irwin 1952):

$$\Delta_{\text{LTTE}} = -\frac{a_{\text{AB}} \sin i_2}{c} \frac{(1 - e_2^2) \sin(v_2 + \omega_2)}{1 + e_2 \cos v_2}, \quad (7)$$

or, changing to eccentric anomaly:

$$\Delta_{\text{LTTE}} = -\mathcal{A}_{\text{LTTE}} \sin(\mathcal{E}_2 + \phi) + \frac{\mathcal{A}_{\text{LTTE}}}{\sqrt{1 - e_2^2 \cos^2 \omega_2}} e_2 \sin \omega_2, \quad (8)$$

where a_{AB} denotes the semi-major axis of the EB’s center of mass around the center of mass of the triple system, while i_2 , e_2 , ω_2 stand for the inclination, eccentricity, and argument of periastron of the relative outer orbit (i.e. the orbit of the third component relative to the center of mass of the EB), respectively. Furthermore, v_2 and \mathcal{E}_2 are the true and eccentric anomalies of the third component, respectively, and c is the speed of light. Note the negative sign on the right hand sides, which arises from the use of the *companion’s* argument of periastron ω_2 , instead of the argument of periastron of the light time orbit of the EB ($\omega_{\text{AB}} = \omega_2 + \pi$). This modification was necessary for the use of the dynamical perturbation terms which are expressed in the orbital elements of the third component’s relative outer orbit (see below). Moreover, the amplitude of the LTTE curve is

$$\mathcal{A}_{\text{LTTE}} = \frac{a_{\text{AB}} \sin i_2}{c} \sqrt{1 - e_2^2 \cos^2 \omega_2}, \quad (9)$$

while its phase ϕ can be calculated as:

$$\phi = \arctan \left(\frac{\sin \omega_2}{\sqrt{1 - e_2^2 \cos^2 \omega_2}} \right). \quad (10)$$

The ETV contribution of the short-period dynamical perturbations (Δ_{dyn}) has a very complicated dependence on the orbital elements of the inner and outer orbits, and their relative configurations as well. Furthermore, for eccentric inner orbits even the orbits’ relative orientation to the observer becomes an additional important factor. The most thorough discussion of these effects can be found in Borkovits et al. (2015). Here, for simplicity, we give only the most dominant terms of the analytic description:

$$\begin{aligned} \Delta_{\text{dyn}}^{\text{lead}} &= \mathcal{A}_{\text{dyn}} (1 - e_1^2)^{1/2} \left\{ \left(1 \mp \frac{3}{2} e_1 \sin \omega_1 \right) \right. \\ &\quad \times \left[\left(1 - \frac{3}{2} \sin^2 i_m \right) \mathcal{M} + \frac{3}{4} \sin^2 i_m \mathcal{S} \right] \\ &\quad \mp \frac{15}{4} e_1 \sin(\omega_1 - 2g_1) \\ &\quad \times \left[\sin^2 i_m \mathcal{M} + \frac{1}{2} (1 + \sin^2 i_m) \mathcal{S} \right] \\ &\quad \left. \pm \frac{15}{4} e_1 \cos(\omega_1 - 2g_1) (1 + \cos i_m) \mathcal{C} \right\} + \mathcal{O}(e_1^2), \end{aligned} \quad (11)$$

where

$$\mathcal{A}_{\text{dyn}} = \frac{1}{2\pi} \frac{m_{\text{C}}}{m_{\text{ABC}}} \frac{P_1^2}{P_2} (1 - e_2^2)^{-3/2}, \quad (12)$$

which, as was found in Borkovits et al. (2016), in most cases, gives a reasonable estimation for the ETV-amplitude of the short-term dynamical contribution. The time-dependence is buried within the trigonometric expressions:

$$\begin{aligned} \mathcal{M} &= v_2 - l_2 + e_2 \sin v_2, & (13) \\ \mathcal{S} &= \sin(2v_2 + 2g_2) + e_2 \left[\sin(v_2 + 2g_2) + \frac{1}{3} \sin(3v_2 + 2g_2) \right], & (14) \\ \mathcal{C} &= \cos(2v_2 + 2g_2) + e_2 \left[\cos(v_2 + 2g_2) + \frac{1}{3} \cos(3v_2 + 2g_2) \right]. & (15) \end{aligned}$$

Moreover, i_m means the mutual (relative) inclination of the inner and outer orbits, while l_2 stands for the mean anomaly of the tertiary and $g_{1,2}$ denote the arguments of periastron of the inner and outer orbits, measured from the intersections of the respective orbital planes and the invariable plane of the triple. Note, in Eq. (11) the upper and lower signs refer to the primary and secondary eclipses, respectively.

Comparing the amplitudes of the LTTE and dynamical terms, Borkovits et al. (2016) showed that they fulfill the inequality:

$$\frac{\mathcal{A}_{\text{dyn}}}{\mathcal{A}_{\text{LTTE}}} \geq 1.45 \times 10^3 m_{\text{ABC}}^{-1/3} \frac{P_1^2}{P_2^{5/3}}, \quad (16)$$

where P ’s should be expressed in days, and m_{ABC} in solar mass. As all of our five triple system member candidate EBs eclipsing periods $P_1 < 4$ days, we can substitute this upper limit into the above equation. Then one can obtain

$$\frac{\mathcal{A}_{\text{dyn}}}{\mathcal{A}_{\text{LTTE}}} \gtrsim m_{\text{ABC}}^{-1/3} \left(\frac{P_1}{4} \right)^2 \left(\frac{416}{P_2} \right)^{5/3}, \quad (17)$$

which illustrates, that the dynamical contribution should be likely larger than, or at least comparable to the LTTE contribution for such short outer period third bodies found in our sample.

The combination of the LTTE and dynamical contributions allows us to calculate both the total mass of the inner

EB and the individual mass of the third component in a dynamical way. This is so, because, similar to the radial velocity solution of a single line spectroscopic binary, the mass function of the distant component C can be calculated from the LTTE component as

$$f(m_C) = m_C \sin^3 i_2 \left(\frac{m_C}{m_{ABC}} \right)^2 = \frac{4\pi^2 a_{AB}^3 \sin^3 i_2}{GP_2^2}. \quad (18)$$

This shows that if the outer mass ratio (m_C/m_{ABC}) and the inclination of the outer orbit (i_2) were known, the mass of the third companion (m_C) and the total mass of the inner EB (m_{AB}) could be calculated. Now the outer mass ratio m_C/m_{ABC} is a direct output of the dynamical contribution, therefore the projected masses $m_{AB} \sin^3 i_2$ and $m_C \sin^3 i_2$ can be immediately calculated from a combined ETV solution. Regarding the outer inclination i_2 , it can be derived e.g. from the expression

$$\sin i_2 = \left| \frac{\sin(\omega_1 - g_1)}{\sin(\omega_2 - g_2)} \right| \sin i_1, \quad (19)$$

where $\omega_{1,2}$, $g_{1,2}$ are direct outputs of the ETV solution, while $\sin i_1$ can be taken from the light curve solution. The verification and detailed discussion of this relationship is given in [Borkovits et al. \(2015, Appendix D\)](#). Note, however that, as it will be discussed in the next section, five of our six ETV solutions resulted in almost coplanar orbits ($i_m < 5^\circ$) and, therefore, for these cases the $\sin i_2 \approx \sin i_1$ approximation would be just as adequate.

As mentioned before, three of the five EBs were found to have eccentric inner orbits. Moreover, for two of them we detected evidences of apsidal motion (see, e.g., [Cowling 1938](#); [Sterne 1939](#); [Gimenez & Garcia-Pelayo 1983](#)), too. Therefore these three systems required the inclusion of the apsidal motion related terms, too, into their ETV analysis, as follows:

$$\Delta_{\text{apse}} = \pm \frac{P_1}{2\pi} \left[2 \arctan \left(\frac{e_1 \cos \omega_1}{1 + \sqrt{1 - e_1^2} \mp e_1 \sin \omega_1} \right) + \sqrt{1 - e_1^2} \frac{e_1 \cos \omega_1}{1 \mp e_1 \sin \omega_1} \right], \quad (20)$$

where, as before, the alternate signs refer again to the primary and secondary eclipses, respectively. Since this expression gives the displacement of the secondary eclipse from photometric phase 0.5, it carries important information on the eccentricity, or, strictly speaking, on the $e_1 \cos \omega_1$ parameter of the EB, even in the absence of any detectable apsidal motion. The apsidal motion of the EB's orbit then is included into Eq. (20) through the time dependence of ω_1 . Our code allows different modes for modelling the apsidal motion. In the present work two of them were applied. In mode AP1 the apsidal motion is considered to be linear in time, i.e. the apsidal advance rate is an additional constant parameter, which is unconstrained, i.e. can be adjusted freely. On the contrary, in mode AP2 it is treated as a fixed quantity calculated internally from the third-body perturbation equations, as described in [Borkovits et al. \(2015, Appendix C\)](#).

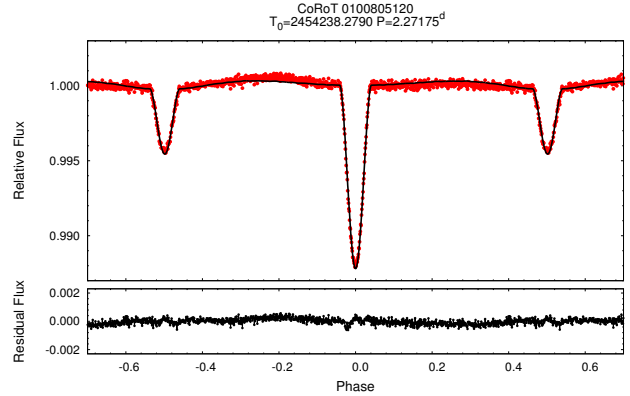


Figure 1. Folded, binned, averaged light curve of CoRoT 100805120 (red) together with the synthesized light curve solution (black) and the residual curve (below).

3 RESULTS

We found five EBs in the whole CoRoT sample for which we were able to establish reliable, physically consistent results. We list the basic parameters of these five EBs in [Table 1](#). (Note, for simplicity, in all the Tables we use reduced BJDs – hereafter RBJD –, i. e. BJD – 2 400 000.) As it can be seen, all of them are relatively short-period, detached binaries. In this section we discuss the complex analysis of each of these ternary system candidates separately, though the numerical results are tabulated collectively in [Tables 2](#) (light curves), [3](#) (ETVs) and [4](#) (derived parameters obtained by the combination of the two kinds of analysis).⁹ We then give a short description of some additional EBs for which, although an ETV solution was not possible, nevertheless, some of their light curve features may imply a multiple nature with various probabilities.

3.1 Hierarchical triple system candidates with consistent ETV and light curve solutions.

CoRoT 100805120. This is an Algol-type EB with $P \approx 2.27$ days period in the CoRoT-LRc01 field ([Cabrerá et al. 2009](#)). The eclipse depths are only $\sim 1.1\%$ and $\sim 0.4\%$ for the primary and secondary minima, respectively. Such small amplitude eclipses with relatively high secondary to primary eclipse depth ratio and long eclipse durations (~ 0.075 in phase) are good indicators of a significant amount of third light in the light curve. Our light curve analysis (see the first column of [Table 2](#), and also [Fig. 1](#)) reveals that only less than 8% of the total flux of the CoRoT light curve comes from the eclipsing pair. (Note, the ExoDat catalog gives only 1.6% contamination rate, therefore the source of the extra light should really be the primary, unresolved CoRoT target.) According to our analysis the EB has a slightly eccentric orbit seen almost along the direction of the major axis. The asymmetric out-of-eclipse section of the folded light curve may also exhibit some rotational modulations.

⁹ The times of minima of the five EBs are tabulated in [Appendix A](#).

Table 1. Properties of the investigated systems. Most of the data, with the exception of the binary ephemerides (i.e. zero epoch – T_0 ; and period – P_1), were taken from the ExoDat Information System. T_0 and P_1 are obtained from our ETV analysis, and may serve as ephemerides for future follow-up observations (see Sect. 4.2 for details).

CoRoT Id	Run(s)	Mag. in R	T_0 RBJD	P_1 [days]	SpT.
100805120	LRc01	12.83	54238.2824(3)	2.271722(8)	K0III
101290947	LRc01	13.74	54237.66574(1)	2.048813(1)	G0III
102698865	LRa01, LRa06	13.99	54398.5431(1)	3.7735657(2)	A0V
104079133	LRc04	15.01	55022.7375(1)	2.764624(5)	G2V
110830711	LRa02	12.85	54789.29970(4)	2.545875(2)	F5V

Table 2. Parameters obtained from the light curve solutions, together with the epoch (T_0) and period (P_1) used for creating the folded light curves. Numbers in parentheses denote 1- σ uncertainties in the last digits. (Parameters without uncertainties were kept on fixed values.)

Parameters	100805120	101290947	102698865 ^b	104079133	110830711
T_0 [RBJD]	54238.2790	54237.6683	54398.6000	55022.73835	54789.2988
P_1 [d]	2.27175	2.04882	3.773576	2.76476830	2.54588
e_1	0.020(7)	0	0.080(3)	0.005(2)	0
ω_1 [deg]	101(2)	–	43(2)	292(9)	–
i_1 [deg]	81.81(9)	88.5(5)	89.0(3)	88.4(1)	88.1(1)
$(\lambda_0)_1^a$ [deg]	269.7(1)	269.98(3)	276.9(3)	270.2(1)	269.993(6)
q_1	0.20(14)	0.93 ^{+0.13} _{-0.55}	0.64(6)	0.34(3)	0.491(1) ^c
r_A	0.205(13)	0.0783(5)	0.1502(7)	0.0840(7)	0.1102(3)
r_B	0.080(13)	0.0763(5)	0.0968(6)	0.0650(7)	0.0547(3)
T_B/T_A	0.784(7)	0.982(3)	0.914(4)	0.800(1)	0.625(2)
$L_A/(L_A + L_B)$	0.95(2)	0.53 ^{+0.02} _{-0.09}	0.775(4)	0.802(4)	0.9637(6)
l_3	0.907(12)	0.907(9)	0.151(8)	0.726(4)	0.06 ^{+0.01} _{-0.03}
$\log g_A^*$	4.04(6)	4.75 ^{+0.08} _{-0.02}	3.93(1)	4.67(1)	4.438(2)
$\log g_B^*$	4.40(1.02)	4.73 ^{+0.04} _{-0.18}	4.17(4)	4.57(8)	4.840(5)

Notes. *a*: True longitude (i.e. $l_0 + \omega_1$) of the secondary component at epoch T_0 ; *b*: monochromatic logarithmic limb-darkening coefficients were adjusted. Results: $x_A = 0.376^{+0.049}_{-0.027}$; $x_B = 0.496^{+0.020}_{-0.013}$; $y_A = 0.277^{+0.058}_{-0.034}$; $y_B = 0.227^{+0.047}_{-0.033}$; *c*: constrained by the formulae of Tout et al. (1996), see text for details.

Table 3. Orbital elements from combined dynamical and LTTE solutions. For eccentric inner EBs the ETV-derived values of the EB's eccentricity (e_1), argument of periastron (ω_1), and apsidal motion period (U) are also given in the notes. (Note U_{fit} and U_{calc} refer to freely adjusted – AP1 – and constrained – AP2 – mode apsidal motion solutions.) Furthermore, for the two non-coplanar solutions (i.e. $i_m > 1^\circ$) the calculated observable inclination (i_2) of the outer orbit, and the sky-projected angular distance of the ascending nodes ($\Delta\Omega = \Omega_2 - \Omega_1$) are also listed in the notes.

CoRoT Id	P_2 (d)	a_2 (R_\odot)	e_2	ω_2 ($^\circ$)	τ_2 (RBJD)	i_m ($^\circ$)	$f(m_C)$ (M_\odot)	$\frac{m_C}{m_{ABC}}$	m_{AB} (M_\odot)	m_C (M_\odot)
100805120 ^a	104(1)	141(10)	0.16(1)	49(4)	54259(2)	0.3 ^{+1.8} _{-0.3}	0.71(10)	0.60(3)	1.38(31)	2.06(44)
101290947	110.2(1)	139(5)	0.350(5)	106(4)	54254.7(1)	0.0(–)	0.109(6)	0.33(1)	1.96(24)	0.98(12)
102698865 ^b	272(1)	315(8)	0.32(4)	103(5)	54272(5)	0.3 ^{+2.4} _{-0.3}	0.04(1)	0.19(2)	4.58(44)	1.09(10)
102698865 ^c	831(34)	679(38)	0.43(14)	343(73)	54456(170)	39(3)	0.11(4)	0.31(5)	4.20(84)	1.88(30)
104079133 ^d	90(2)	108(5)	0.20(2)	349(2)	55047.4(6)	0.9(6)	0.12(5)	0.39(7)	1.28(21)	0.81(20)
110830711 ^e	82(2)	108(6)	0.119(8)	14(2)	54754(2)	4.9 ^{+5.2} _{-1.3}	0.04(2)	0.25(5)	1.87(36)	0.62(13)

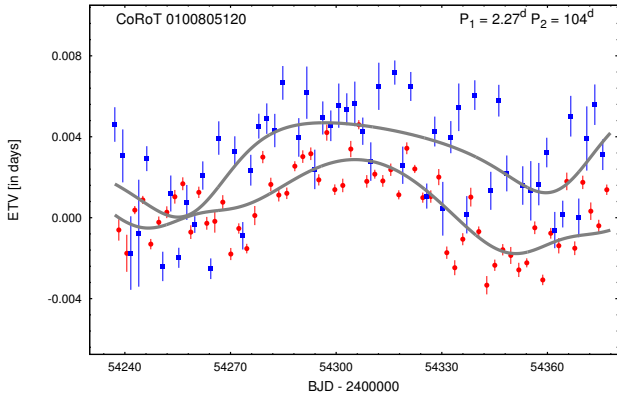
Notes. *a*: $e_1 = 0.026(3)$; $\omega_1 = 91.2(6)^\circ$; $U_{\text{calc}} = 28$ yr; *b*: $e_1 = 0.078(6)$; $\omega_1 = 41(3)^\circ$; $U_{\text{fit}} = 279(39)$ yr; *c*: $e_1 = 0.100(3)$; $\omega_1 = 54(2)^\circ$; $U_{\text{fit}} = 415(22)$ yr; $\Delta\Omega = -24(7)^\circ$; $i_2 = 58(9)^\circ$; *d*: $e_1 = 0.0040(6)$; $\omega_1 = 300(4)^\circ$; $U_{\text{fit}} = 2.4(7)$ yr; Conjunctions of the outer orbit (in RBJD): $t_{\text{inf}} = 55033(1)$, $t_{\text{sup}} = 55067(1)$; *e*: $\Delta\Omega = -2(7)^\circ$; $i_2 = 92(4)^\circ$.

The ETVs of both the primary and secondary minima show sinusoidal features and furthermore, the slight divergence between the two curves might be indicative of apsidal motion. Therefore, we were looking for combined LTTE+dynamical ETV solution, allowing apsidal motion, too. We made runs both with freely adjusted (i.e. unconstrained – mode AP1, see Borkovits et al. 2015, Sect. 2.2)

and dynamically constrained (mode AP2) apsidal advance rates. As the unconstrained solution resulted in an apsidal advance rate close to the constrained one, we kept the latter, constrained solution. The model ETV curves (together with the observed ETVs) are plotted in Fig. 2, while the main parameters of our solutions are listed in the first row of Table 3. Note that, in addition of the direct output parameters

Table 4. Physical parameters of the eclipsing binaries from the combination of the light curve and ETV solutions.

CoRoT Id	a_1 (R_\odot)	m_A (M_\odot)	m_B (M_\odot)	R_A (R_\odot)	R_B (R_\odot)
100805120	8.1(6)	1.15(29)	0.23(14)	1.66(16)	0.65(12)
101290947	8.5(3)	1.01 $^{+0.31}_{-0.14}$	0.94 $^{+0.13}_{-0.31}$	0.67(2)	0.65(2)
102698865	16.9(5)	2.79(29)	1.79(20)	2.54(8)	1.64(5)
102698865	16.4(1.1)	2.56(52)	1.64(34)	2.47(17)	1.59(11)
104079133	9.1(5)	0.95(16)	0.32(6)	0.76(4)	0.59(3)
110830711	9.7(6)	1.25(24)	0.61(12)	1.07(7)	0.53(3)

**Figure 2.** Primary (red points) and secondary (blue rectangles) ETV curves of CoRoT 100805120 together with the combined LTTE+dynamical ETV solution (grey).

of the ETV solution, we also listed the the derived masses of the outer binary, i.e. m_{AB} and m_C , in the last two columns.

According to our solution the inner and outer orbits are almost coplanar, which is in good agreement with the fact that no eclipse depth variations were detected during the ~ 141 -day-long CoRoT observations.

Considering the masses, we found $m_C > m_{AB}$; that is, the third component seems to be the most massive object in the triple. Therefore, it should probably be the brightest star in the system, unless it was a degenerate object. Its derived mass $m_C = 2.1 \pm 0.4 M_\odot$ is in good agreement with the spectral classification of K0III which is given in the ExoDat catalog. Although our solution gives only the total mass ($m_{AB} = 1.4 \pm 0.3 M_\odot$) of the inner, eclipsing binary, with the use of the photometric mass ratio¹⁰ $q_1 = 0.2 \pm 0.1$ obtained from the light curve solution above, one can get the individual masses of the two stars forming the inner EB. Furthermore, combining the physical dimensions of the semi-major axis of the EB's orbit deduced from the ETV solution with the fractional radii, one can calculate the stellar radii in physical units, too. We tabulate these derived values in

¹⁰ Note, that Borkovits et al. (2015) showed that the mass ratio q_1 of the EB can also be determined from the dynamical ETV analysis when the terms higher order in the period ratio (P_1/P_2) were considered, too. In the present study, however, for the shortness of the data series and their limited accuracy (at least relative to the measurements of the prime *Kepler* mission) we decided not to include these terms.

Table 4. This way we can give another rough estimation for the expected amount of the photometric third light (l_3). According to our results, the primary component of the EB might be a moderately evolved solar-like star. Taking therefore the crude estimation $T_{\text{eff},A} = 6000 \pm 500$ K, and using $R_A = 1.7 \pm 0.2 R_\odot$ (see Table 4), we get $L_A = 3.4 \pm 1.4 L_\odot$. Assuming that the third component is really a K0III star, its luminosity is expected to be in the range $25 \lesssim L_C \lesssim 100 L_\odot$ (see, e.g. Kumar et al. 2011) and therefore, one can get $0.83 \lesssim l_3 \approx L_C / (L_A + L_B + L_C) \lesssim 0.98$. This result is in good agreement with the amount of the third light found in our light curve analysis. Thus, we conclude, that this triple candidate could join the still few-membered club of *Kepler*-spacecraft discovered compact hierarchical triple systems, in which the distant tertiary component is a red giant star (e.g. HD 181068 – Drekas et al. 2011; Borkovits et al. 2013, KIC 07690843 – Gaulme et al. 2013; Borkovits et al. 2016, KIC 07955301 – Rappaport et al. 2013; Gaulme et al. 2013).

CoRoT 101290947 is another, ~ 2 day-period detached binary in the LRc-01 field, with almost equally shallow primary and secondary eclipses (with a depth of 3.5%, see Fig. 3). Its eclipsing nature was first reported by (Cabrera et al. 2009). Moreover, the large amplitude, sine-like ETV has also been noticed and interpreted as LTTE by the same group but, apart from a conference poster, their findings have remained unpublished (Cabrera, 2016, private communication). Our light curve solution (second column in Table 2) has resulted in an eclipsing pair seen almost edge-on, formed by two very similar stars, and a huge $l_3 \approx 90\%$ third flux contribution, $\sim 10 - 11\%$ of which – according to ExoDat – may arise from resolved contaminating sources. Therefore, similar to the previous system, the spectral information given in previous works cannot be used for discussing the fundamental physical properties of the binary.¹¹ Considering, however, the obtained surface gravity indicators ($\log g_{A,B}^* = 4.7$), we may assume that the binary is composed of two low-mass main-sequence stars.¹² Finally, we note that the residual light curve shows a systematic sine-like structure of the order ~ 1000 ppm. This feature may come from rotational modulation (see bottom panel of Fig. 3).

Turning to the ETV analysis, for the circular inner orbit we used the average of equally good quality primary and secondary ETV curves for our analysis. (The advantages of the use of averaged ETVs were discussed in Borkovits et al. 2016.) Our first runs with freely adjusted mutual inclinations resulted in a solution with a mutual inclination $i_m = 21.5^{+3.6}_{-7.8}$. We found, however, that all the physically realistic configurations in this mutual inclination range would

¹¹ For this system ExoDat and Sarro et al. (2013) contradict each other. The former gives spectral classification G0III, while the latter gives $\log g = 4.6$, which suggest luminosity class V (i.e. main-sequence star).

¹² A little caution is needed here on the accurate values of the two strongly correlated quantities of the third light (l_3) and the inclination (i_1). Our $\log g_{A,B}^*$ values would suggest either very low-mass or undersized main-sequence components. Despite the fact that the obtained i_1 and l_3 values were found to be very similar and robust in all Markov Chains, we cannot exclude the possibility that this result might have been affected by the evident out-of-eclipse distortions, and the true inclination and third flux may be somewhat lower and therefore, the radii of the stars a bit larger.

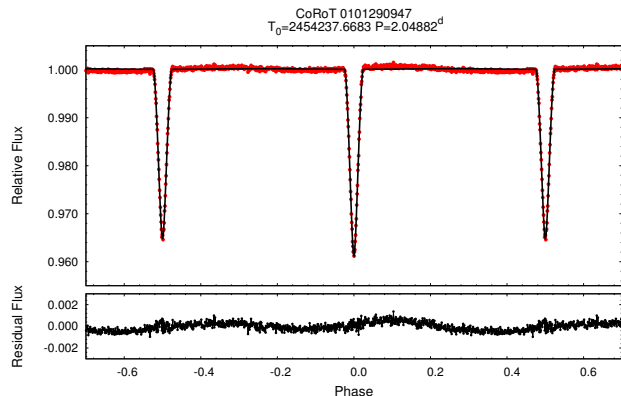


Figure 3. Folded, binned, averaged light curve of CoRoT 101290947 (red) together with the synthesized light curve solution (black) and the residual curve (below). The small systematic residuals may be the manifestation of rotational modulations due to chromospheric activity.

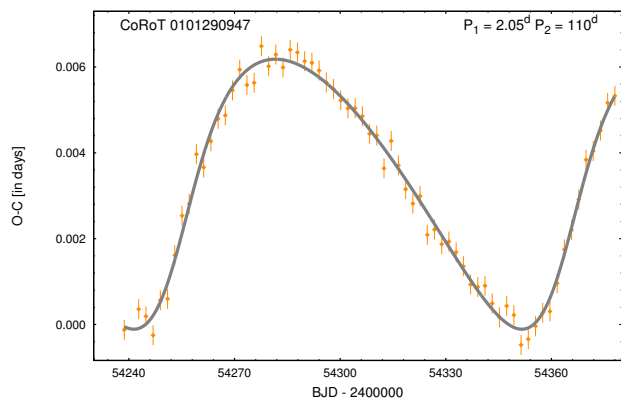


Figure 4. Timing curve for the averaged ETV data of CoRoT 101290947 together with the combined LTTE+dynamical solution for coplanar configuration.

have resulted in fast inclination variations ($\Delta i_1 \sim \pm 1 - 2^\circ$) during the four months of CoRoT observations. Such a large inclination variation would have given rise to remarkable eclipse depth variations, which was not observed. Therefore we omitted these models, and fixed $i_m = 0^\circ$. Our coplanar solution is tabulated in the second row of Table 3 (see also Fig. 4), while the derived individual masses and physical radii of the EB components are given in Table 4. According to our solution the three stars would have similar masses around $\sim 0.9 - 1.0 M_\odot$. Some caution, however, is necessary, as in this case the EB members would be remarkably undersized. On the other hand, the similar mass of the tertiary did not necessarily contradict to the large amount of the third light. This question may be resolved by assuming either that the third component – again – is a red giant star, or that part of the extra light comes from a fourth, unresolved source, not necessarily binned to the triple.

CoRoT 102698865. This is the longest period ($P_1 \sim 3^d 77$) EB in our sample, and the only one observed by the spacecraft during two different runs. The datasets LRA1 and

LRA6 cover ~ 131 and ~ 77 days respectively, with a gap of cca. ~ 1410 days between the two. The light curve exhibits total eclipses with primary transits and secondary occultations, the latter being slightly displaced from phase 0^h5 (Fig. 5).

As before, first we carried out the analysis of the phase-folded, averaged light curve. The analysis resulted in a significant, but nevertheless not dominant third light ($l_3 \approx 15 - 20\%$). (The contamination rate tabulated in ExoDat catalog is 0.5%.) Therefore in this case we assumed that the spectral classification (A0V) given in the ExoDat catalog indeed refers to the primary of the eclipsing pair, thus its temperature, bolometric albedo and surface gravity exponent were set accordingly. Despite the correctly set limb-darkening and other atmospheric parameters our solutions failed in the sense that we were not able to model the eclipses better than with ~ 5000 ppm residuals. Such, relatively higher light curve residuals were found by other authors too for the high-accuracy *Kepler*- and CoRoT light curves. The possible reasons, including the not fully adequate physical models of the stellar atmospheres, were discussed briefly by Hambleton et al. (2013). Therefore, similar to, e.g. Southworth et al. (2011), we decided to adjust the (logarithmic) limb-darkening coefficients, too. As result a substantially improved solution was obtained, tabulated in Table 2, and plotted in Fig. 5. Our result is in agreement with this spectral classification, as we found ($\log g_A^* = 3.93 \pm 0.01$) which, substituting the typical mass of a main-sequence, early A-type star, gives a surface gravity about $\log g_A \approx 4.10$ corresponding to this spectral type.

Considering the ETVs, the primary and secondary curves clearly converge to each other, which is an evidence of the apsidal motion. Furthermore, the slopes and the curvatures of the curves are very different in the two observing runs. Consequently, the presence of a third star, perturbing the motion of the EB is a reasonable assumption. On the other hand, however, the two segments of the ETVs do not show evident periodicities, which makes the period of the third body, and thus, any quantitative ETV solutions less certain. Therefore, it is not surprising that, instead of a unique solution, we found two similarly acceptable third body configurations, with substantially different outer periods.¹³ We tabulate the results of both solutions in the third and fourth rows of Tables 3 and 4, and plot them in the two panels of Fig. 6. While in the case of the shorter outer period solution the two orbits were found to be practically coplanar, the other solution resulted in a higher mutual inclination $i_m = 39 \pm 3^\circ$. The angle between the ascending nodes of the two orbits was found to be $\Delta\Omega = \Omega_2 - \Omega_1 = -24 \pm 7^\circ$, which results in an observable inclination of $i_2 = 58 \pm 10^\circ$ for the outer orbit. This solution predicts an inclination variation of $\Delta i_1 \approx 0.2$ for the 1617-day long interval between the first and the last CoRoT data points, which, due to the total eclipses, remains below the limit of the observable eclipse depth variations. Furthermore, the obtained masses for the binary members in both solutions are in good agreement

¹³ Strictly speaking, a third set of formal third-body solutions was also found in the outer period range $P_2 \sim 1100 - 1300$ days, but these solutions resulted in astrophysically unrealistic stellar masses and therefore, in what follows, we do not consider them.

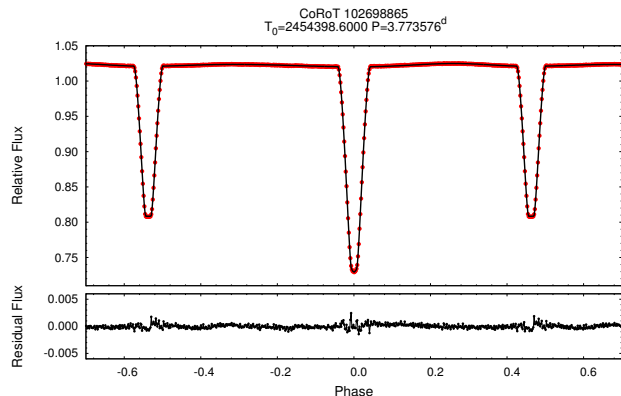


Figure 5. Folded, binned, averaged light curve of CoRoT 102698865 (red) together with the synthesized light curve solution (black) and the residual curve (below).

with the results of the light curve analysis. Comparing the obtained amount of third light $l_3 = 0.15 \pm 0.01$ with the mass of the third component ($m_C = 1.1 \pm 0.1 M_\odot$ and $1.9 \pm 0.3 M_\odot$ for the shorter and longer outer period solutions, respectively), one can see, that for the second solution this value is in perfect agreement with the expected contribution of a main-sequence tertiary with the given mass, while for the first case the third star might be an evolved object or, some additional sources should also be assumed.

CoRoT 104079133 is another marginally eccentric detached EB with a period of $P_1 \sim 2^d7$ and moderately differing eclipse depths (see Fig. 7), observed during the run LRc04. The most exciting features of the light curve are the two groups of extraneous eclipses with various shapes about BJDs 2 455 031-32 and 2 455 065-66 (see Fig. 8) which makes it very likely that CoRoT 104079133 belongs to the small group of triply eclipsing hierarchical triple systems. According to our light curve solution (Table 2) the extra flux dominates ($l_3 \approx 72\%$) the CoRoT observations. (The outer contamination rate, given in ExoDat, is about $\sim 2\%$.) Therefore, we may expect again, that the spectral informations given in ExoDat does not refer to the EB members, but to the source of the extra flux.

We were looking again for a combined LTTE+dynamical ETV solution. Due to the marginal eccentricity of the inner EB we decided to take into account both the primary and secondary ETVs despite the fact that the latter data had significantly larger uncertainties. Naturally, this also implies the inclusion of the apsidal motion terms into our analysis. Our results (see Fig. 9) are tabulated in the fifth rows of Tables 3 and 4. The most important finding is that the moments of the inferior and superior conjunctions of the EB and the third component relative to the Earth ($t_{\text{inf}} = 55033 \pm 1$ RBJD and $t_{\text{sup}} = 55067 \pm 1$ RBJD) are in very good agreement with the locations of the extra eclipses in the light curve. This makes it very likely that the ETV and the outer eclipses are caused by the same object.

From the locations of the extra eclipses relative to the two kinds of conjunctions points, one can make a few simple, qualitative statements on the geometry of the extra eclipses. Thus, given that the first set of the extra eclipses (consist-

ing of two individual fadings, see the left panel of Fig. 8) occurred around the inferior conjunction, i.e. when the third object was located between the Earth and the EB, it shows the tertiary component eclipsing the members of the inner binary. As the first event did happen after a primary eclipse of the EB, in the case of (almost) coplanar orbits with prograde revolutions (i.e. $i_m = 0^\circ9 \pm 0^\circ6$), the primary component was eclipsed first, while during the second, shallower fading, which occurred before the forthcoming secondary eclipse, the secondary star was eclipsed.

A more complex structure of three extraneous events of the second group of the extra eclipses can be seen in the right panel of Fig. 8. These events were observed close to the superior conjunction. Therefore, here the EB members eclipsed the third star. The first, long-duration event occurred just before a secondary eclipse, therefore, here the secondary component should have been the eclipser. The eclipse duration was necessarily longer, because the secondary, in its revolution around the primary of the EB was moving in these moments in almost the opposite direction to the revolution in the outer orbit. Then, just after the mid-time of the secondary eclipse, the primary component also eclipsed the tertiary. Due to the similarly directed revolution of the primary on both the inner and outer orbits at those moments, this event was the shortest. Finally, just after the quadrature position of the inner EB, the secondary component eclipsed again the tertiary star. A more detailed, quantitative light curve analysis of this triple star, capable of resolving the ambiguity of prograde vs. retrograde revolution, is planned in a future work.

Considering the masses obtained, our combined analysis resulted in similar masses for the primary and tertiary components ($m_A = 0.95 \pm 0.16 M_\odot$ and $m_C = 0.81 \pm 0.20 M_\odot$, respectively), and a less massive secondary star ($m_B = 0.32 \pm 0.06 M_\odot$). While the masses of both the primary and the tertiary are in agreement with the spectral class G5V given in the ExoDat catalog, there is a slight discrepancy with the high amount of the third light ($l_3 = 0.726 \pm 0.004$). This fact emphasizes again the importance of a further, more detailed analysis.

CoRoT 110830711 was observed during run LRa02. The Algol-type light curve of this $P \sim 2^d55$ -binary shows relatively deep ($\sim 25\%$) primary transits and shallow ($\sim 2\%$) secondary occultations. The out-of-eclipse sections exhibit strong quasi-sinusoidal modulations with an amplitude similar to the depths of the secondary eclipses. These modulations remain clearly visible in the folded, binned averaged light curve (see Fig. 10), suggesting rotational origin with a synchronized primary stellar spin rate. Not being our primary interest, for the light curve analysis they were simply modeled mathematically as an extra flux component of the form $\Delta\phi = a \cos(2\pi/P \cdot t) + b \sin(2\pi/P \cdot t)$, where the coefficients a and b were determined with a linear least-squares fitting for each trial set (of light curve parameters) during the MCMC search. The resulting parameters are tabulated in the last column of Table 2, while the synthesized light curve (and the residuals, with and without the extra trigonometric terms) are plotted in Fig. 10. As it can be seen, the extra flux is almost negligible in this case ($l_3 \approx 3 - 7\%$), therefore one can assume that the spectral classification (F5V) given in ExoDat refers to the primary component of the EB. Note that our first solutions with freely adjusted mass ratio re-

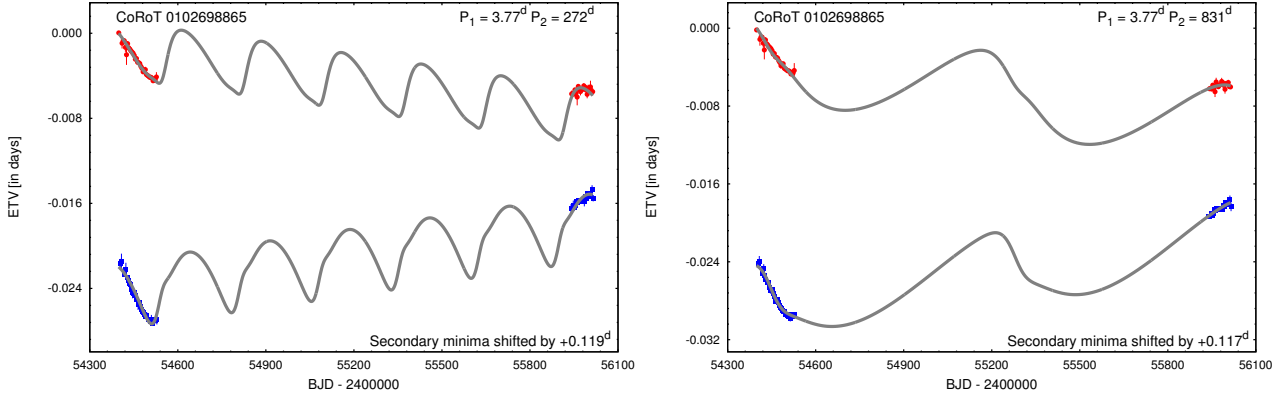


Figure 6. ETVs of primary (red) and secondary (blue) minima of CoRoT 102698865 together with two different combined LTTE+dyn ETV solutions (grey). In case of the shorter outer period solution (left) the convergence of the two curves reveals relatively rapid apsidal motion. (Note, the secondary curves are upshifted by $\sim 0^{\text{d}}.12$ for better visibility.)

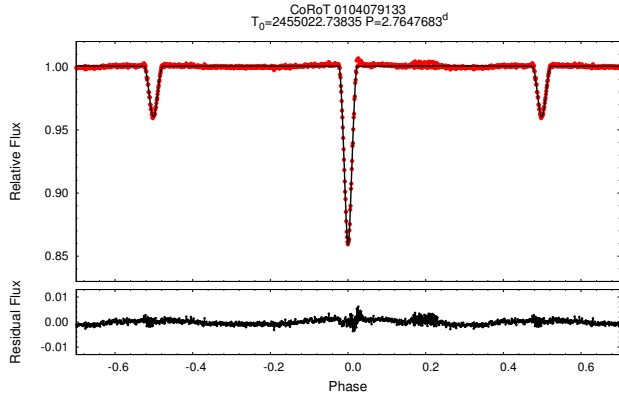


Figure 7. Folded, binned, averaged light curve of CoRoT 104079133 (red) together with the synthesized light curve solution (black) and the residual curve (below).

sulted in unrealistically low mass ratios of $q_1 \sim 0.002 - 0.008$. But, as we have emphasized previously, the photometric mass ratio is known to be an ill-determined quantity for detached systems. Therefore we resorted to another kind of constraining the mass ratio, with the combination and inversion of the zero age main-sequence mass–luminosity and mass–radii relations of [Tout et al. \(1996\)](#), in the same way as Sect. 7 of [Rappaport et al. \(2017\)](#) did. (To do this, the effective temperature of the primary was set to $T_{\text{eff1}} = 7120$ K, conforming to its spectral type.) Then, comparing the minima of the χ^2 values of the freely adjusted and constrained-q chains, the difference was about 1.4%, while all the values of the other parameters remained within the uncertainties given in Table 2. Hence we conclude that the extreme mass ratio found in our first MCMC analysis is probably false, and the binary most probably consists of two normal main-sequence stars, but with quite different masses.

Turning to the ETV solution, we used only the ETV curve of the primary eclipses, and omitted the secondary ETV curve obtained with a substantially larger scatter from the shallow secondary eclipses. Our combined LTTE+dynamical solution, which has the shortest outer period ($P_2 = 82 \pm 2$ d) in our sample, is tabulated in the last row

of Table 3 and plotted in Fig. 11. According to our results, the two orbits are slightly misaligned ($i_m = 4^{\circ}9^{+5}_{-1.3}$). Therefore one can expect a precession of the EB’s orbital plane with an amplitude of $\sim 4 - 10^{\circ}$ on a timescale of $\sim 20 - 40$ years (see, e.g. [Borkovits et al. 2015](#), for a detailed discussion on the orbital precession induced by a third star on misaligned orbit). Considering the individual stellar masses deduced from the combination of the light curve and ETV solutions (last row in Table 4), the mass of the primary ($m_A = 1.25 \pm 0.24 M_{\odot}$) within its 1σ uncertainty, is in agreement with the expected mass of an *F5V* star. The secondary and tertiary components were found to have similar masses ($m_B = 0.61 \pm 0.12 M_{\odot}$ and $m_C = 0.62 \pm 0.13 M_{\odot}$, respectively). The expected light contribution of such a less massive star is also in good agreement with the small amount of the third light ($I_3 = 0.06^{+0.01}_{-0.03}$).

3.2 Systems with extra eclipse(s), but without detectable ETVs.

We identified some additional CoRoT EBs where extra eclipsing event(s) can be found in the light curve, but do not show detectable third-body signals in their ETV. Among them the most promising hierarchical triple candidate is the SRa02 target CoRoT 221664856. In this case the complex characteristics of the three extraneous eclipsing events at BJD 2 454 768–2 454 770 (Fig. 12) clearly reveal the triply eclipsing hierarchical triple nature of this system. Unfortunately, the short (~ 33 -day-long) dataset does not make it possible to get any reasonable ETV solution. Therefore, ground based photometric follow-up observations of this system in the future would be exceptionally worthy. Note, however, that the spectral classification of G2I given in the ExoDat site cannot refer to any of the stars of the inner pair, as it is not possible for such large supergiant stars to form a well-detached $\sim 2^{\text{d}}06$ -day-period close binary with any other star. Therefore, if the given luminosity class was valid, the supergiant star should be the tertiary component.

We have also identified four new blended EBs (i.e. mixed light curves of two EBs without any detectable interactions between them) in the CoRoT fields. (Note, blended light curves of CoRoT 211625668 – [Erikson et al. 2012](#) and

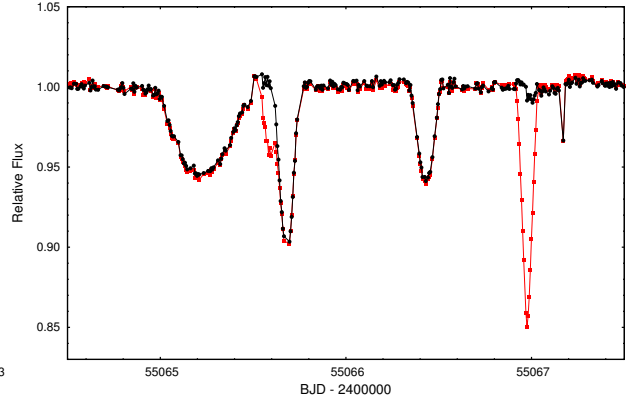
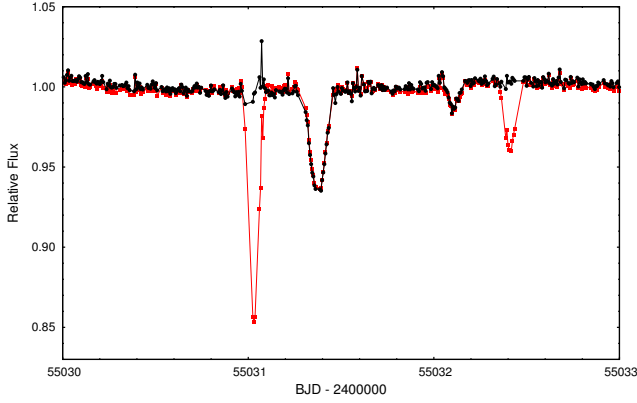


Figure 8. The extra eclipsing events on the observed, detrended light curve of CoRoT 104079133 (red). The black curve represents the residual light curve obtained after the interpolated removal of the phase-folded, averaged light curve from the observed, detrended curve. The complex characteristics of the extra eclipses make it certain that CoRoT 104079133 is (at least) a triply eclipsing hierarchical triple system.

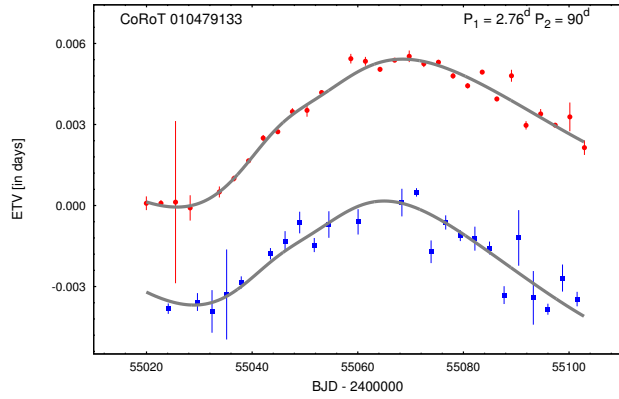


Figure 9. Eclipse timing diagrams of primary (red) and secondary (blue) eclipses of CoRoT 104079133 system together with the accepted LTTE+dynamical ETV solution (grey).

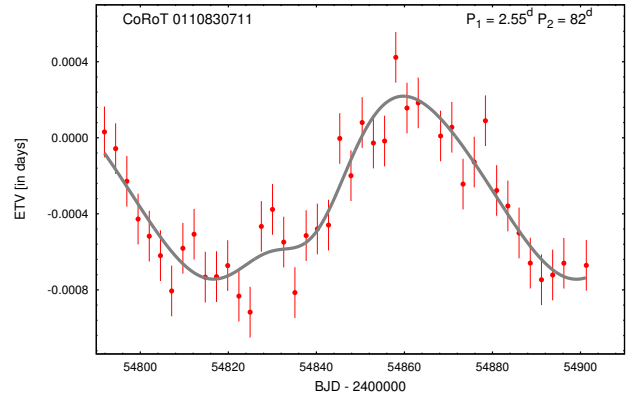


Figure 11. ETV of the primary minima in CoRoT 110830711 and the combined LTTE+dynamical solution curve.

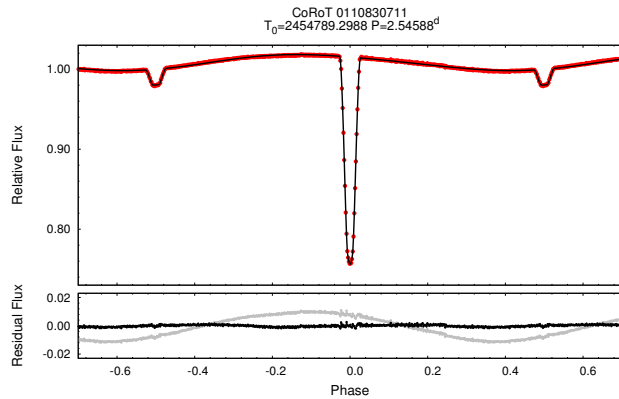


Figure 10. Folded, binned, averaged light curve of CoRoT 110830711 (red) together with the synthesized light curve solution (black). Note, the out-of-eclipse modulation was modelled mathematically with an extra sinusoidal term (see text for details). In the lower panel the residual curves are shown with and without the extra sinusoidal term (black and grey curves, respectively).

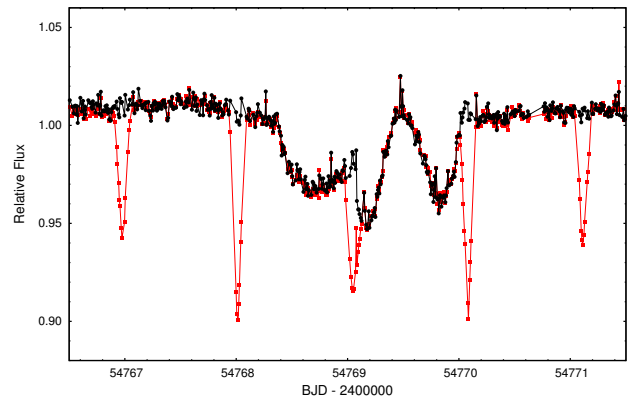


Figure 12. The extra eclipsing events on the observed, detrended light curve of CoRoT 221664856 (red). The black curve represents the residual light curve obtained after the interpolated removal of the phase-folded, averaged light curve from the observed, detrended curve. The complex characteristics of the extra eclipses make it certain that CoRoT 221664856 is at least a triply eclipsing hierarchical triple system.

CoRoT 310266512 – Fernández Fernández & Chou 2015 were reported previously.) For these systems the light curves can be easily disentangled into pairs of separate EBs, and the ETVs do not exhibit any short-term interactions. Therefore we cannot decide whether these systems are hierarchic 2+2 multiples with long outer periods, or unbounded EBs seen in the same direction. We list these systems in Table 5 and plot their light curves in Figs. 13–16.

Interestingly, at least five of these eight EBs have eccentric orbits. Amongst them, the binary CoRoT 110829335B, one of the longest period EBs in the whole CoRoT sample ($P_B \approx 50^d31$), has extremely displaced secondary minima ($\phi_{\text{IB}} \approx 0^{\circ}91$), therefore, its eccentricity should be $e_B \gtrsim 0.71$.¹⁴ Note, the eccentricity of its ($P_A \approx 8^d93$ -day-period) blended mate, i.e. CoRoT 110829335A should also exceed $e_{A,\text{min}} \approx 0.41$.

The light curve of the SRa01 target CoRoT 211659387 is formed by the blend of a $P_A \approx 0^d39$ -day-period overcontact and a $P_A \approx 4^d00$ -day-period detached EB¹⁵ (Fig. 14). As one can see, the period ratio is almost $\sim 1:10$. According to the ExoDat site, however, the contamination ratio of this source is about 55%. We made some *VRI*-band photometric follow-up observations of this interesting blended source on the nights of 21/22, 23/24, 24/25 and 26/27 August, 2015 with the 90/60cm Schmidt telescope located on the Piszkes-tető Mountain Station of the Konkoly Observatory. Our observations cover the full phase of the short period overcontact component (denoted with green cross in Fig. 17). We plot also the phase-folded *I*-band light curve in the left panel of Fig. 14. As one can see, the 2015 light curve folded with the ephemeris determined from the CoRoT measurements (obtained in 2007) shows significant shift in phase which cannot be explained by the uncertainty of the period determination, but imply real variation(s) in the eclipsing period (which might be either physical or apparent). On the other hand, unfortunately, we were not able to observe any light curve variations (practically, eclipses) coming from the longer period binary component. Therefore, further observations are urgently needed.

Another new, interesting blended system is CoRoT 223993566 which was observed during both the SRa01 and SRa05 runs. Therefore the full length of the data window is almost 4 years, which made it possible to detect evidence of apsidal motion (i.e. slight convergence of the primary and secondary ETV curves) in the $P_A \approx 1^d18$ -day-period eccentric binary A. The other, shorter period ($P_B \approx 0^d93$) EB in this blended system is likely to have circular orbit, and exhibits a remarkable reflection/irradiation effect (see the right panel of Fig. 15).

Finally, the composite light curve of CoRoT 310284765 exhibits the mixture of the light curves of two short-period, slightly eccentric Algols (Fig. 16).

Table 5. Orbital ephemerides of the newly identified blended CoRoT EBs.

CoRoT id	T_0 (RBJD)	P (d)	Remark
110829335	54795.4332	8.9304	$\phi_{\text{I}} = 0^{\circ}247$
	54818.7400	50.3075	$\phi_{\text{I}} = 0^{\circ}909$
211659387	54204.1360	0.393957	
	54204.7450	4.00	
223993566	54533.8317	1.18067	$\phi_{\text{I}} = 0^{\circ}483^a$
	54534.3098	0.934856	strong reflection
310284765	54927.2249	2.371125	$\phi_{\text{I}} = 0^{\circ}587$
	54927.0710	1.8754	$\phi_{\text{I}} = 0^{\circ}522$

4 DISCUSSION

4.1 Comparison with compact *Kepler*-triples

Despite the fact that the group of the tight hierarchical triple star candidates presented above in the CoRoT sample are not nearly as numerous as in the *Kepler*-sample, and the quantitative results obtained above are naturally far less certain than in the latter case, we conclude our study with some qualitative comparison with the findings of Borkovits et al. (2016) on the *Kepler*-sample. For this we plotted in Fig. 18 the six possible configurations found for our five triple candidates on the $P_1 - P_2$ plane together with the *Kepler*-triples having, according to the results of Borkovits et al. (2016), inner and outer periods $P_1 \leq 10$ d and $P_2 \leq 1000$ d, respectively. As it can be seen (shaded yellow region in Fig. 18), similar to the *Kepler*-sample, we did not find any short outer period triple amongst the shortest period EBs, which practically means the lack of tight third stellar components revolving around overcontact systems. The absence of such systems from the *Kepler*-sample was first noticed by Conroy et al. (2014). Our results emphasize again that this effect should have an astrophysical (more probably evolutionary) origin.

Turning to our five candidate systems, four of them have inner periods between 2 and 3 days. The sample of Borkovits et al. (2016) contains 17 triple candidates having inner periods in the same domain. The shortest outer period in the *Kepler*-sample is $P_2 = 515$ d. There are, however, 7 triple candidates amongst the $P_2 < 2$ d inner period systems in the *Kepler*-sample, the outer periods of which remain $P_2 < 110$ d. The lack of systems with similar outer periods in the same inner period domain suggests that our results should be taken with a grain of salt. It is possible that the analysed ETVs cover only smaller portions of the outer orbits instead of almost a full cycle and, therefore, the orbital solutions might be misinterpreted, and the true outer period might be substantially longer. On the other hand, taking into account the low overall population of the $P_2 < 2 - 300$ d region itself, the absence of such short outer period systems in the $2 \lesssim P_1 \lesssim 4$ d inner period regime from the *Kepler* data could be a purely statistical fluctuation. Consequently, the observed distribution difference does not necessarily question the validity of our solutions.

¹⁴ For the extremely high eccentricity, we calculated e_{min} by the use of the *complete, analytical form* of the time displacement, i.e. Eq. (20), instead of its frequently used first order (in eccentricity) approximation related simply to $e \cos \omega$.

¹⁵ Interestingly, Erikson et al. (2012) give ephemeris for this latter, detached binary in their Table 10 without mentioning the 0^d39 -day overcontact component.

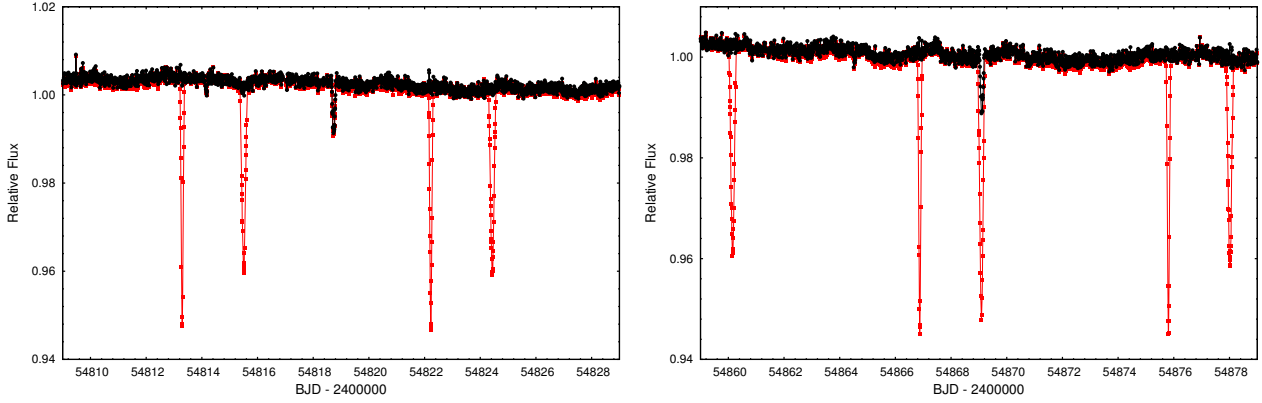


Figure 13. The extra eclipsing events on the observed, detrended light curve of CoRoT 110829335 (red). The black curve represents the residual light curve obtained after the interpolated removal of the phase-folded, averaged light curve from the observed, detrended curve. The two sets of a shallow fading (secondary eclipse of binary B) followed regularly by a somewhat deeper other fading (primary eclipse in binary B) reveal the two-EB blended nature of the light curve.

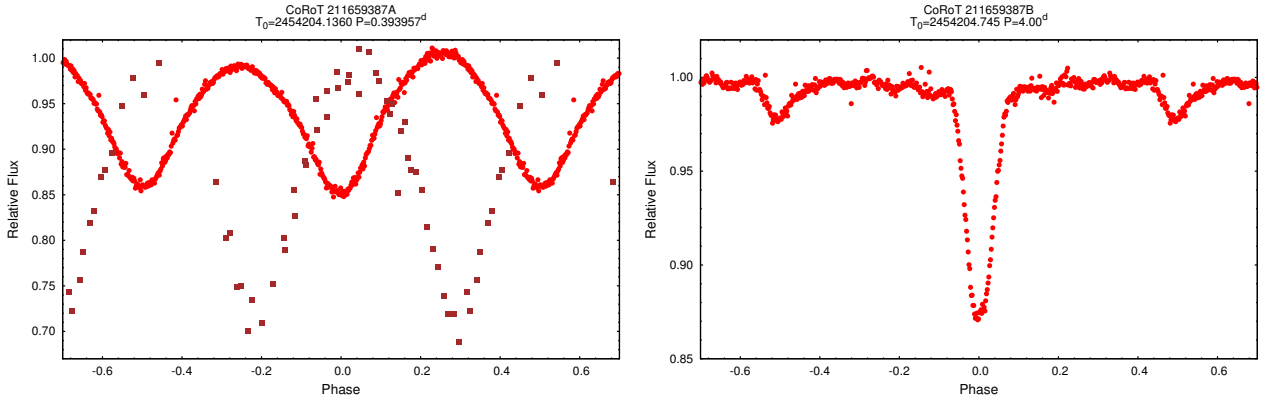


Figure 14. The disentangled, folded, binned, averaged light curves of the two EBs blended in the light curve of the CoRoT target id. 211659387. Note the period ratio of the two EBs are very close to 1 : 10. This seems to be an incidental fact. In the left panel we plotted also (with brown boxes) the folded light curve formed from our (*I*-band) ground-based follow up observations on four nights at August 2015 at Piskésetető Observatory, Hungary. As it can be seen, the orbital phases has shifted by almost a quarter of the eclipsing period by the time of our observations, which cannot be explained with the uncertainty of the calculated eclipsing period, but imply some period variations (being either physical or apparent, incidental or continuous) since the epoch of the CoRoT measurements.

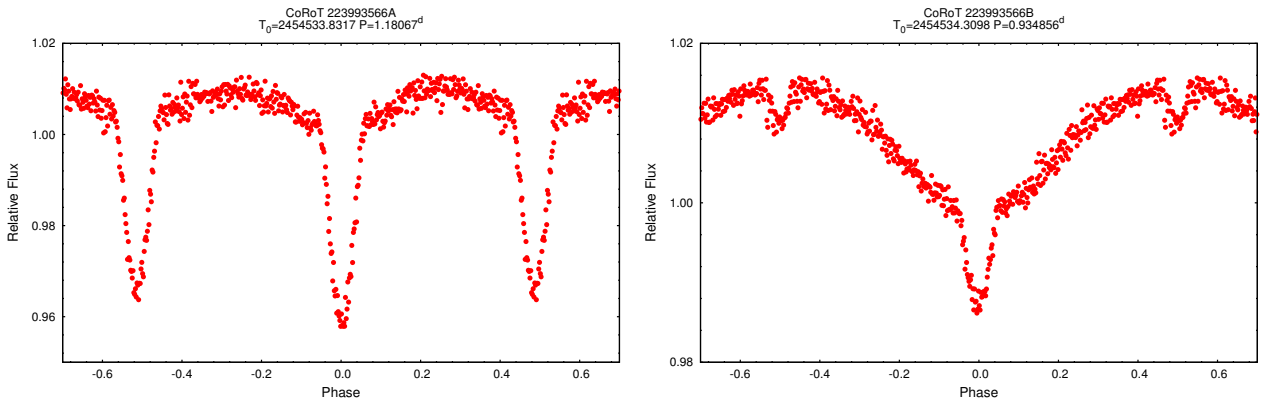


Figure 15. The disentangled, folded, binned, averaged light curves of the two EBs blended in the light curve of the CoRoT target id. 223993566. Note the remarkable reflection/irradiation effect in the second binary.

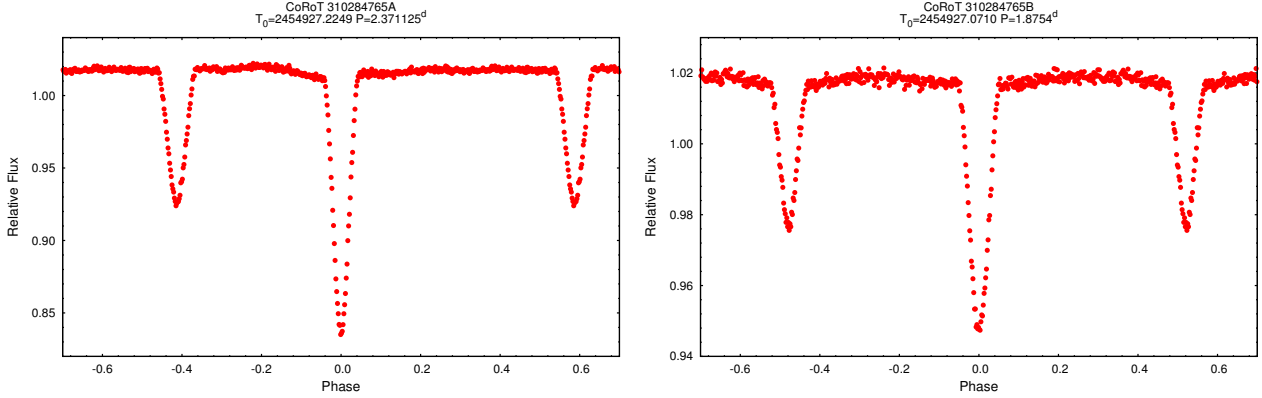


Figure 16. The disentangled, folded, binned, averaged light curves of the two EBs blended in the light curve of the CoRoT target id. 310284765. Note, both EBs have slightly displaced secondary minima, indicating eccentric orbits.

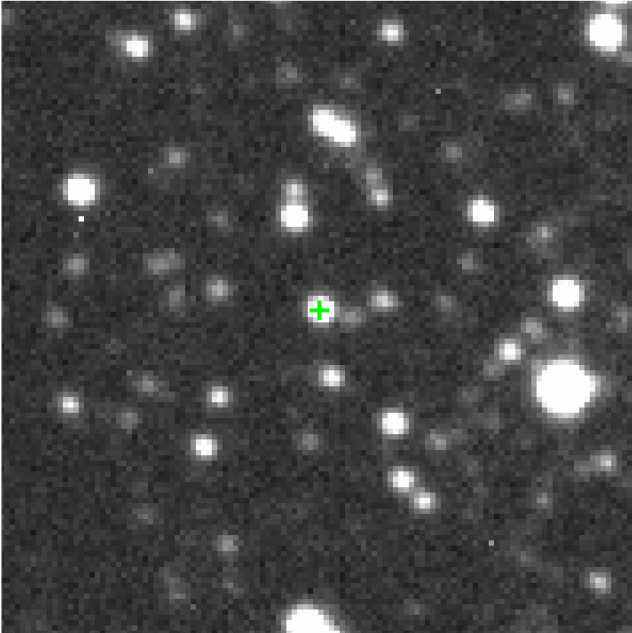


Figure 17. A narrow 2'x2'-section of the field of view around the CoRoT target id. 211659387. The photo was taken with the 90/60cm Schmidt telescope of Konkoly Observatory. The source of the overcontact EB-light curve is matched with green cross. No brightness variations exceeding a 3σ -level were found for the other closest objects which contaminated probably the CoRoT measurements.

4.2 Prospects of ground-based follow-up observations

It is evident that further observations are needed to clarify (or refute) our findings. Therefore, in what follows, we briefly discuss the possibilities of future, ground-based follow-up observations. First we consider the spectroscopic measurements. Our candidates are relatively faint, but they would still be available with several instruments equipped to relatively large (3+m aperture) telescopes. For two of the three third-light dominated systems (CoRoT 100805120 and CoRoT 101290947) we can expect to detect only the lines of the more distant tertiary components (which are most

probably red giants). Nevertheless, the determination of the parameters of the outer orbits (including the spectroscopic mass functions) from radial velocity measurements would allow us to lift the high-degree degeneracy between the LTTE and dynamical contributions of the ETV solution (see the discussion in Rappaport et al. 2013) and, therefore, would enable us to calculate an accurate dynamical model, including a reliable dynamical mass determination. For the remaining third-light dominated system, the triply eclipsing CoRoT 104079133, one can expect to detect both the lines of the primary component of the inner EB, and the tertiary star. Because of the chance of being an SB3 system, CoRoT 102698865 could be the most promising triple candidate, while CoRoT 11083077 is expected to be an SB1 system. Note, due to the 3-4 month-long (short) outer periods of all but one of our triple candidates, the spectroscopic outer orbits could be determined during one observing session with the exception of CoRoT 102698865. Multi-session observations, however, would also be preferred for the systems with shorter outer periods in order to detect the effects of the longer time-scale three-body perturbations on the orbit(s).

As for the possibility of photometric follow-up observations, which are the most common way of obtaining additional eclipsing minima time measurements over time for ETV studies, our systems are exposed to both favourable and very unfavourable circumstances. Although the short period of the majority of our systems (including other systems, discussed in subsection 3.2, too) would be ideal for such observations, the combination of the very small eclipse depths (at least in the third-flux dominated systems) with the low amplitude ETVs may pose too great a challenge for the earth-based measurements. For example in the case of CoRoT 100805120 and CoRoT 101290947 a millimagnitude photometric accuracy of each individual measurement would be required for a satisfactory signal to noise ratio. On the other hand, the situation is more mixed for the case of CoRoT 110830711: although its primary minima with amplitudes exceeding $0^m.2$ magnitudes can be observed with satisfactory photometric accuracy even with smaller telescopes and in average sky conditions, the full amplitude of the ETV curve is only about $0^d.001$ -day, which requires an accuracy of some 10^{-4} days for each time of minimum determination.

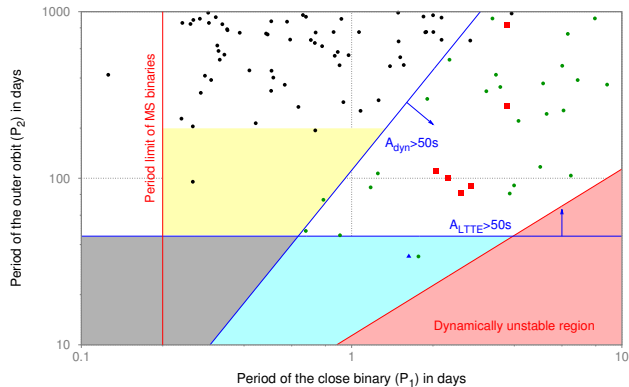


Figure 18. The location of the five triple star candidates (red boxes) on the P_1 vs P_2 plane. (The two alternative third-body solutions for CoRoT 102698865 are plotted separately.) For a comparison we plotted those short-period *Kepler*-triple system candidates for which the inner and outer periods are $P_1 \leq 10$ d and $P_2 \leq 1000$ d. Following the work of Borkovits et al. (2016), the pure LTTE systems are marked with black circles, while triples with combined LTTE+dynamical ETV solution are plotted with green. Furthermore, the first triple system discovered during the K2 mission (HD 144548 – Alonso et al. 2015) is also plotted (blue triangle). The blue lines show the borders of the domains where the amplitudes of the LTTE and dynamical terms may exceed ~ 50 sec, which can be regarded as a limit for an unambiguous detection. These limits were calculated for a hypothetical triple system of three, equally solar mass stars, with a typical outer eccentricity of $e_2 = 0.35$, and quite arbitrarily, $i_2 = 60^\circ$ and $\omega_2 \pm 90^\circ$. The shaded areas have the following meanings: (i) grey: in this region no LTTE or dynamical perturbations are detectable at all via ETV analysis; (ii) cyan: no LTTE can be detected, though dynamical effect may be significant and, therefore, certainly detectable; (iii) yellow: the “desert” of close (but clearly LTTE-detectable) third companions around short period EBs (mostly overcontact systems); red: dynamically unstable region, in the sense of the stability criterium of Mardling & Aarseth (2001). (See text for further details.)

In this respect the two most promising targets would be CoRoT 102698865 and CoRoT 104079133, having both relatively deep primary eclipses and larger ETV amplitudes at the same time. Furthermore, in the first of them the apsidal motion could also be well followed with ground-based minima observations, while in the latter one the detection of probable future outer eclipses offers a further exciting possibility. This latter statement also holds for CoRoT 221664856. However, one should keep in mind that the outer eclipse events may last as long as one or two days, meaning that a successful observation of such events would require international campaigns in the future, similar to the one organized by Conroy et al. (2015) for the observation of the forecasted outer eclipse of KIC 02835289.

5 SUMMARY AND CONCLUSIONS

In this paper we reported the results of our search for close, third stellar companions to eclipsing binaries observed with CoRoT spacecraft via ETV, as well as some auxiliary light curve analyses. Despite the short length of the data series,

we were able to find third-body solutions (with combination of light-travel time effect and third-body perturbations) for ETV curves of five, relatively short-period Algol-systems, namely the CoRoT ids. 100805120, 101290947, 102698865, 104079133, and 110830711. The periods of the outer orbits were found to be between 82 and 831 days. For one of them, CoRoT 102698865, we obtained two alternative solutions with outer periods of 272 and 831 days, respectively. Apsidal motion (most probably of dynamical origin) was also detected for three eccentric systems. For three of the five systems the light curve is dominated by the extra (third) flux, suggesting that the spectral information available in the literature for these systems refer to the source of the extra flux rather than the EB itself. By combining the results of the light curve and ETV analyses we were able to calculate in a dynamical manner the individual masses of all the three components and the physical dimensions of the inner EB’s stellar components as well. These results, though with relatively higher uncertainties, are consistent with both the available spectral information and the amounts of extra lights deduced from the light curve solutions. Our results support that CoRoT 100805120 (and perhaps CoRoT 101290947) join the still small group of compact hierarchical triple stars with red giants as their most massive component.

We have identified two EBs exhibiting extraneous eclipses with complex structures. These certain triply eclipsing triple systems are CoRoTs 104079133 and 221664856. For the first system extra eclipses both around the inferior and superior conjunctions were observed, and we were also able to obtain ETV solution (see the previous paragraph). For the second system the short dataset covering only 1 month was insufficient to provide any meaningful ETV solution.

We have also reported four new composite light curves of blended EBs. Five of the eight blended EBs revolve on eccentric orbits and one of them, CoRoT 110829335B, was found to be extremely eccentric with $e \geq 0.71$, while the sixth blended EB, CoRoT 223993566B, exhibits remarkable reflection/irradiation effect.

Finally, we discuss briefly the reliability of our ETV solutions. Their fundamental weakness is that they do not satisfy the most natural criterion of a trustworthy three-body interpretation of an ETV curve, which states that the observations should cover at least two outer orbital periods (e.g. Conroy et al. 2014; Borkovits et al. 2016). On the other hand, the solutions for these triple candidates fulfill the first three criteria of Frieboes-Conde & Herczeg (1973). Note, however that, with the extra information obtainable from a combined LTTE + dynamical solution in our hand, we can slightly reformulate and strengthen the original criteria, listed in the Introduction, at some points. Therefore, in our case we can state that we were able to model the timing data of the selected EBs with combined LTTE+dynamical ETV three-body models (i.e. criterion 1), fitting simultaneously the primary and secondary curves (2). From the ETV solutions we derived the total masses (m_{AB}) of the inner EBs and the masses (m_C) of the third components, which were found to be consistent with the amounts of the third lights (I_3), obtained from the auxiliary light curve analyses (3). (Note that the last criterion of Frieboes-Conde & Herczeg (1973) cannot be applied on our systems due to the lack of

radial velocity observations.) Finally, in the case of the triply eclipsing system CoRoT 104079133 we have also found that the extra eclipses were occurred in the vicinity of the inferior and superior conjunction points of the outer orbit of the ETV solution, which makes it very likely that the source of the ETV signal is identical with the outer eclipsing component, strengthening our confidence regarding the reliability of our ETV solution based third-body model.

Therefore, we may conclude that, despite the short data lengths compared to the periods of the detected outer orbits, our solutions were found to be physically consistent and, therefore, the third-body hypotheses seem to be well established. Further observations, however, are necessary to confirm and refine, or refute, our results.

ACKNOWLEDGEMENTS

This project has partly been supported by the HAS Wigner RCP - GPU-Lab and the Hungarian National Research, Development and Innovation Office, NKFIH-OTKA grants K-113117 and K-115709. This research has made use of the ExoDat Database, operated at LAM-OAMP, Marseille, France, on behalf of the CoRoT/Exoplanet program. This research has made use of data collected by the CoRoT mission. The research has also made use of the VizieR catalogue access tool, CDS, Strasbourg, France. The original description of the VizieR service was published by [Ochsenbein et al. \(2000\)](#). The authors are grateful to the referee, K. Conroy, for his valuable comments and suggestions which helped us to substantially improve the quality of the paper, and to G. Kutrovat and I. B. Biro for the linguistic corrections.

REFERENCES

Alonso R., Deeg H. J., Hoyer S., Lodieu N., Palle E., Sanchis-Ojeda R., 2015, *A&A*, **584**, L8
 Auvergne M., et al., 2009, *A&A*, **506**, 411
 Baglin A., et al., 2006, in 36th COSPAR Scientific Assembly.
 Balaji B., Croll B., Levine A. M., Rappaport S., 2015, *MNRAS*, **448**, 429
 Baudin F., Maceroni C., Alencar S. H. P., 2016, IV.3 The wealth of stellar variability. p. 209, doi:10.1051/978-2-7598-1876-1.c043
 Borkovits T., Erdi B., Forgacs-Dajka E., Kovacs T., 2003, *A&A*, **398**, 1091
 Borkovits T., Csizmadia S., Forgacs-Dajka E., Hegedus T., 2011, *A&A*, **528**, A53
 Borkovits T., et al., 2013, *MNRAS*, **428**, 1656
 Borkovits T., et al., 2014, *MNRAS*, **443**, 3068
 Borkovits T., Rappaport S., Hajdu T., Sztakovics J., 2015, *MNRAS*, **448**, 946
 Borkovits T., Hajdu T., Sztakovics J., Rappaport S., Levine A., Biro I. B., Klagyivik P., 2016, *MNRAS*, **455**, 4136
 Borucki W. J., et al., 2010, *Science*, **327**, 977
 Cabrera J., et al., 2009, *A&A*, **506**, 501
 Chaintreuil S., Deru A., Baudin F., Ferrigno A., Grolleau E., Romagnan R., 2016, II.4 The "ready to use" CoRoT data. p. 61, doi:10.1051/978-2-7598-1876-1.c024
 Chandler S. C., 1888, Bulletin Astronomique, Serie I, **5**, 499
 Conroy K. E., Prsa A., Stassun K. G., Orosz J. A., Fabrycky D. C., Welsh W. F., 2014, *AJ*, **147**, 45
 Conroy K., Prsa A., Stassun K., Orosz J., 2015, Information Bulletin on Variable Stars, **6138**

Cowling T. G., 1938, *MNRAS*, **98**, 734
 Deleuil M., et al., 2009, *AJ*, **138**, 649
 Derezak A., et al., 2011, *Science*, **332**, 216
 Erikson A., et al., 2012, *A&A*, **539**, A14
 Fabrycky D., Tremaine S., 2007, *ApJ*, **669**, 1298
 Fernandez Fernandez J., Chou D.-Y., 2015, *PASP*, **127**, 421
 Frieboes-Conde H., Herczeg T., 1973, *A&AS*, **12**, 1
 Gaulme P., McKeever J., Rawls M. L., Jackiewicz J., Mosser B., Guzik J. A., 2013, *ApJ*, **767**, 82
 Gies D. R., Matson R. A., Guo Z., Lester K. V., Orosz J. A., Peters G. J., 2015, *AJ*, **150**, 178
 Gimenez A., Garcia-Pelayo J. M., 1983, *Ap&SS*, **92**, 203
 Hambleton K. M., et al., 2013, *MNRAS*, **434**, 925
 Irwin J. B., 1952, *ApJ*, **116**, 211
 Irwin J. B., 1959, *AJ*, **64**, 149
 Kirk B., et al., 2016, *AJ*, **151**, 68
 Kiseleva L. G., Eggleton P. P., Mikkola S., 1998, *MNRAS*, **300**, 292
 Klingsmith D. A., Sobieski S., 1970, *AJ*, **75**, 175
 Kumar Y. B., Reddy B. E., Lambert D. L., 2011, *ApJ*, **730**, L12
 Mardling R. A., Aarseth S. J., 2001, *MNRAS*, **321**, 398
 Mayer P., 1990, Bulletin of the Astronomical Institutes of Czechoslovakia, **41**, 231
 Naoz S., Fabrycky D. C., 2014, *ApJ*, **793**, 137
 Naoz S., Fragos T., Geller A., Stephan A. P., Rasio F. A., 2016, *ApJ*, **822**, L24
 Ochsenbein F., Bauer P., Marcout J., 2000, *A&AS*, **143**, 23
 Perets H. B., Fabrycky D. C., 2009, *ApJ*, **697**, 1048
 Prsa A., Zwitter T., 2005, *ApJ*, **628**, 426
 Rappaport S., Deck K., Levine A., Borkovits T., Carter J., El Mellah I., Sanchis-Ojeda R., Kalomeni B., 2013, *ApJ*, **768**, 33
 Rappaport S., et al., 2017, *MNRAS*, **467**, 2160
 Rouan D., Baglin A., Copet E., Schneider J., Barge P., Deleuil M., Vuillemin A., Leger A., 1998, Earth Moon and Planets, **81**, 79
 Sarro L. M., et al., 2013, *A&A*, **550**, A120
 Shappee B. J., Thompson T. A., 2013, *ApJ*, **766**, 64
 Soderhjelm S., 1975, *A&A*, **42**, 229
 Southworth J., Zucker S., Maxted P. F. L., Smalley B., 2004, *MNRAS*, **355**, 986
 Southworth J., et al., 2011, *MNRAS*, **414**, 2413
 Sterken C., 2005, in Sterken C., ed., Astronomical Society of the Pacific Conference Series Vol. 335, The Light-Time Effect in Astrophysics: Causes and cures of the O-C diagram. p. 3
 Sterne T. E., 1939, *MNRAS*, **99**, 451
 Tauris T. M., van den Heuvel E. P. J., 2014, *ApJ*, **781**, L13
 Tokovinin A., 2004, in Allen C., Scarfe C., eds, Revista Mexicana de Astronomia y Astrofisica Conference Series Vol. 21, Revista Mexicana de Astronomia y Astrofisica Conference Series. pp 7–14
 Tokovinin A., 2014, *AJ*, **147**, 87
 Tokovinin A., Thomas S., Sterzik M., Udry S., 2006, *A&A*, **450**, 681
 Tout C. A., Pols O. R., Eggleton P. P., Han Z., 1996, *MNRAS*, **281**, 257
 Tran K., Levine A., Rappaport S., Borkovits T., Csizmadia S., Kalomeni B., 2013, *ApJ*, **774**, 81
 Woltjer Jr. J., 1922, Bull. Astron. Inst. Netherlands, **1**, 93

Table A1. Times of minima of CoRoT 100805120

Time (RBJD)	Cycle no.	std. dev. (<i>d</i>)	Time (RBJD)	Cycle no.	std. dev. (<i>d</i>)	Time (RBJD)	Cycle no.	std. dev. (<i>d</i>)
54237.146244	-0.5	0.000484	54284.855460	20.5	0.000417	54332.559937	41.5	0.000316
54238.276918	0.0	0.000200	54285.985888	21.0	0.000148	54333.689369	42.0	0.000150
54239.416462	0.5	0.000627	54287.131227	21.5	0.000354	54334.833181	42.5	0.000529
54240.547533	1.0	0.000296	54288.258995	22.0	0.000137	54335.962548	43.0	0.000141
54241.683430	1.5	0.000777	54289.396303	22.5	0.000361	54337.099641	43.5	0.000453
54242.821438	2.0	0.000131	54290.531240	23.0	0.000128	54338.236396	44.0	0.000148
54243.956181	2.5	0.001031	54291.670284	23.5	0.000625	54339.377322	44.5	0.000446
54245.093709	3.0	0.000139	54292.803150	24.0	0.000152	54340.506463	45.0	0.000128
54246.231633	3.5	0.000384	54293.938262	24.5	0.000493	54341.655812	45.5	0.000500
54247.363295	4.0	0.000138	54295.073629	25.0	0.000134	54342.775583	46.0	0.000159
54248.512360	4.5	0.000550	54296.212573	25.5	0.000342	54343.916132	46.5	0.000366
54249.636145	5.0	0.000135	54297.347735	26.0	0.000150	54345.048339	47.0	0.000141
54250.769848	5.5	0.000343	54298.483956	26.5	0.000333	54346.192355	47.5	0.000420
54251.908411	6.0	0.000130	54299.616685	27.0	0.000129	54347.320875	48.0	0.000136
54253.045220	6.5	0.000376	54300.756720	27.5	0.000392	54348.460530	48.5	0.000357
54254.180943	7.0	0.000122	54301.888663	28.0	0.000143	54349.592363	49.0	0.000162
54255.313813	7.5	0.000296	54303.028314	28.5	0.000404	54350.723338	49.5	0.000332
54256.453357	8.0	0.000137	54304.162229	29.0	0.000133	54351.863418	50.0	0.000144
54257.588317	8.5	0.000400	54305.300347	29.5	0.000362	54353.003473	50.5	0.000463
54258.722736	9.0	0.000159	54306.435202	30.0	0.000141	54354.135536	51.0	0.000131
54259.858996	9.5	0.000330	54307.570767	30.5	0.000366	54355.274980	51.5	0.000355
54260.996471	10.0	0.000141	54308.704172	31.0	0.000131	54356.409038	52.0	0.000126
54262.133187	10.5	0.000364	54309.841034	31.5	0.000417	54357.547080	52.5	0.000420
54263.266710	11.0	0.000151	54310.976296	32.0	0.000140	54358.678231	53.0	0.000145
54264.400351	11.5	0.000312	54312.116524	32.5	0.000379	54359.820410	53.5	0.000458
54265.538578	12.0	0.000171	54313.247733	33.0	0.000143	54360.952306	54.0	0.000122
54266.678577	12.5	0.000425	54314.390893	33.5	0.000535	54362.088349	54.5	0.000368
54267.811294	13.0	0.000183	54315.520056	34.0	0.000135	54363.223458	55.0	0.000164
54268.955192	13.5	0.000353	54316.660742	34.5	0.000378	54364.360909	55.5	0.000364
54270.080501	14.0	0.000148	54317.790585	35.0	0.000142	54365.498407	56.0	0.000156
54271.221441	14.5	0.000450	54318.927932	35.5	0.000388	54366.637514	56.5	0.000369
54272.353532	15.0	0.000148	54320.064655	36.0	0.000148	54367.766874	57.0	0.000155
54273.489057	15.5	0.000363	54321.203593	36.5	0.000417	54368.904260	57.5	0.000456
54274.624308	16.0	0.000144	54322.335402	37.0	0.000139	54370.041899	58.0	0.000141
54275.764066	16.5	0.000353	54323.467666	37.5	0.000462	54371.179952	58.5	0.000482
54276.897710	17.0	0.000150	54324.605754	38.0	0.000125	54372.312244	59.0	0.000153
54278.038013	17.5	0.000325	54325.741717	38.5	0.000393	54373.453391	59.5	0.000432
54279.172369	18.0	0.000141	54326.877578	39.0	0.000139	54374.583291	60.0	0.000128
54280.310154	18.5	0.000381	54328.016675	39.5	0.000349	54375.722690	60.5	0.000418
54281.442787	19.0	0.000139	54329.150308	40.0	0.000136	54376.856843	61.0	0.000140
54282.581336	19.5	0.000399	54330.284630	40.5	0.000480	54377.990420	61.5	0.000387
54283.714030	20.0	0.000129	54331.418343	41.0	0.000146			

APPENDIX A: TABLES OF TIMES OF MINIMA FOR THE FIVE ANALYSED SYSTEMS

In this Appendix we tabulate (in Tables A1–A5) the individual minima times of the primary and secondary eclipses for the five EBs analysed in Sect. 3.1.

Table A2. Times of minima of CoRoT 101290947

Time (RBJD)	Cycle no.	std. dev. (<i>d</i>)	Time (RBJD)	Cycle no.	std. dev. (<i>d</i>)	Time (RBJD)	Cycle no.	std. dev. (<i>d</i>)
54237.664345	0.0	0.000136	54285.819733	23.5	0.000100	54332.937739	46.5	0.000102
54238.691992	0.5	0.000153	54286.843417	24.0	0.000111	54333.960702	47.0	0.000098
54239.712795	1.0	0.000195	54287.867778	24.5	0.000104	54334.986409	47.5	0.000125
54241.764243	2.0	0.000171	54288.892845	25.0	0.000095	54336.009693	48.0	0.000101
54242.789330	2.5	0.000214	54289.916369	25.5	0.000185	54337.033980	48.5	0.000156
54243.809338	3.0	0.000237	54290.940862	26.0	0.000065	54338.058765	49.0	0.000128
54244.839577	3.5	0.000401	54291.965491	26.5	0.000108	54339.082601	49.5	0.000135
54245.860059	4.0	0.000128	54292.989790	27.0	0.000096	54340.107498	50.0	0.000098
54246.884222	4.5	0.000195	54294.014191	27.5	0.000068	54341.131670	50.5	0.000166
54247.911246	5.0	0.000280	54295.037985	28.0	0.000101	54342.155977	51.0	0.000073
54248.934356	5.5	0.000280	54296.062574	28.5	0.000124	54343.180189	51.5	0.000118
54249.958775	6.0	0.000139	54297.087141	29.0	0.000090	54344.204196	52.0	0.000106
54250.984407	6.5	0.000177	54298.111220	29.5	0.000152	54345.228730	52.5	0.000132
54252.007605	7.0	0.000147	54299.135127	30.0	0.000131	54346.253046	53.0	0.000066
54253.034024	7.5	0.000139	54300.160342	30.5	0.000228	54347.277621	53.5	0.000090
54254.057975	8.0	0.000230	54301.183593	31.0	0.000142	54348.302294	54.0	0.000086
54255.084080	8.5	0.000144	54302.208552	31.5	0.000093	54349.326276	54.5	0.000142
54256.106618	9.0	0.000169	54303.232914	32.0	0.000143	54350.350159	55.0	0.000087
54257.132911	9.5	0.000288	54304.257115	32.5	0.000114	54351.374618	55.5	0.000118
54258.156915	10.0	0.000258	54305.281609	33.0	0.000104	54352.398490	56.0	0.000109
54259.182723	10.5	0.000135	54306.305817	33.5	0.000127	54353.423787	56.5	0.000079
54260.206253	11.0	0.000155	54307.330000	34.0	0.000085	54354.447537	57.0	0.000142
54261.230979	11.5	0.000221	54308.354612	34.5	0.000172	54355.472712	57.5	0.000220
54262.254950	12.0	0.000293	54309.377971	35.0	0.000123	54356.496855	58.0	0.000130
54263.280628	12.5	0.000106	54310.403464	35.5	0.000161	54357.521976	58.5	0.000106
54264.304673	13.0	0.000109	54311.427224	36.0	0.000121	54358.545687	59.0	0.000100
54265.329571	13.5	0.000118	54312.450731	36.5	0.000144	54359.570417	59.5	0.000088
54266.353985	14.0	0.000098	54313.475550	37.0	0.000094	54360.595315	60.0	0.000120
54267.378598	14.5	0.000116	54314.500992	37.5	0.000142	54361.619942	60.5	0.000155
54268.402493	15.0	0.000136	54315.524518	38.0	0.000093	54362.644580	61.0	0.000136
54269.428514	15.5	0.000149	54316.549024	38.5	0.000205	54363.669371	61.5	0.000095
54270.452001	16.0	0.000123	54317.572424	39.0	0.000082	54364.694482	62.0	0.000099
54271.477196	16.5	0.000092	54318.597368	39.5	0.000118	54365.719097	62.5	0.000102
54272.501680	17.0	0.000170	54319.621211	40.0	0.000187	54366.742601	63.0	0.000086
54273.525393	17.5	0.000159	54320.645228	40.5	0.000071	54367.768854	63.5	0.000092
54274.549739	18.0	0.000094	54321.670242	41.0	0.000121	54368.793323	64.0	0.000133
54275.574562	18.5	0.000093	54322.694492	41.5	0.000094	54369.817711	64.5	0.000123
54276.598997	19.0	0.000101	54323.718548	42.0	0.000111	54370.842836	65.0	0.000131
54277.624756	19.5	0.000115	54324.742314	42.5	0.000104	54371.867285	65.5	0.000169
54278.647709	20.0	0.000069	54325.766584	43.0	0.000122	54372.891139	66.0	0.000287
54279.672781	20.5	0.000110	54326.791675	43.5	0.000078	54373.916472	66.5	0.000087
54280.696598	21.0	0.000079	54327.815501	44.0	0.000091	54374.941461	67.0	0.000085
54281.721854	21.5	0.000087	54328.839829	44.5	0.000078	54375.965606	67.5	0.000069
54282.745718	22.0	0.000089	54329.864088	45.0	0.000130	54376.990141	68.0	0.000126
54283.769996	22.5	0.000108	54330.888834	45.5	0.000106	54378.015104	68.5	0.000073
54284.794378	23.0	0.000095	54331.912850	46.0	0.000123			

Table A3. Times of minima of CoRoT 102698865

Time (RBJD)	Cycle no.	std. dev. (<i>d</i>)	Time (RBJD)	Cycle no.	std. dev. (<i>d</i>)	Time (RBJD)	Cycle no.	std. dev. (<i>d</i>)
54398.608096	0.0	0.000094	54472.047495	19.5	0.000051	55949.537829	411.0	0.000074
54400.352100	0.5	0.000088	54474.076262	20.0	0.000052	55951.294555	411.5	0.000104
54404.127336	1.5	0.000107	54475.820765	20.5	0.000040	55953.311804	412.0	0.000063
54407.901090	2.5	0.000057	54477.849641	21.0	0.000050	55955.068274	412.5	0.000059
54409.927825	3.0	0.000100	54479.594185	21.5	0.000042	55957.085055	413.0	0.000063
54411.674986	3.5	0.000088	54481.622876	22.0	0.000082	55958.842228	413.5	0.000062
54413.701646	4.0	0.000083	54483.367611	22.5	0.000045	55960.858257	414.0	0.000058
54415.448825	4.5	0.000082	54485.396617	23.0	0.000045	55962.615712	414.5	0.000071
54417.475185	5.0	0.000072	54487.141003	23.5	0.000044	55964.632828	415.0	0.000081
54419.220562	5.5	0.000064	54489.170217	24.0	0.000067	55966.389493	415.5	0.000060
54421.248132	6.0	0.000063	54490.914422	24.5	0.000055	55968.406117	416.0	0.000050
54422.994651	6.5	0.000160	54492.943320	25.0	0.000053	55970.163013	416.5	0.000058
54425.021002	7.0	0.000145	54494.688024	25.5	0.000061	55972.179471	417.0	0.000079
54426.767475	7.5	0.000104	54496.716803	26.0	0.000058	55973.936551	417.5	0.000060
54428.795605	8.0	0.000059	54498.461234	26.5	0.000053	55975.953188	418.0	0.000064
54430.540713	8.5	0.000060	54500.490291	27.0	0.000062	55977.710169	418.5	0.000067
54432.568783	9.0	0.000063	54502.234783	27.5	0.000058	55979.726835	419.0	0.000070
54434.313957	9.5	0.000043	54504.263756	28.0	0.000064	55981.483771	419.5	0.000073
54436.342227	10.0	0.000053	54506.008214	28.5	0.000045	55983.500711	420.0	0.000069
54438.087481	10.5	0.000051	54508.037328	29.0	0.000061	55985.257240	420.5	0.000121
54440.115633	11.0	0.000064	54509.781938	29.5	0.000054	55987.274157	421.0	0.000069
54441.860534	11.5	0.000050	54511.810821	30.0	0.000046	55989.031257	421.5	0.000055
54443.889083	12.0	0.000055	54513.555162	30.5	0.000059	55991.047439	422.0	0.000072
54445.633825	12.5	0.000042	54515.584129	31.0	0.000057	55992.804643	422.5	0.000085
54447.662532	13.0	0.000055	54517.328917	31.5	0.000037	55994.820608	423.0	0.000143
54449.407340	13.5	0.000043	54519.357722	32.0	0.000050	55996.578636	423.5	0.000090
54451.435896	14.0	0.000049	54521.102481	32.5	0.000040	55998.594774	424.0	0.000076
54453.180993	14.5	0.000049	54523.131364	33.0	0.000064	56000.351969	424.5	0.000056
54455.209106	15.0	0.000060	54524.876093	33.5	0.000059	56002.369950	425.0	0.000268
54456.954225	15.5	0.000047	54526.905187	34.0	0.000070	56004.125615	425.5	0.000081
54458.982738	16.0	0.000039	54528.649795	34.5	0.000058	56006.142000	426.0	0.000074
54460.727426	16.5	0.000057	55939.973721	408.5	0.000065	56007.899256	426.5	0.000062
54462.755950	17.0	0.000051	55941.990731	409.0	0.000071	56009.915150	427.0	0.000060
54464.500540	17.5	0.000086	55943.747292	409.5	0.000054	56011.673261	427.5	0.000070
54466.529478	18.0	0.000053	55945.764353	410.0	0.000066	56013.688681	428.0	0.000060
54468.274289	18.5	0.000047	55947.521194	410.5	0.000068	56015.446049	428.5	0.000070
54470.302961	19.0	0.000063						

Table A4. Times of minima of CoRoT 104079133

Time (RBJD)	Cycle no.	std. dev. (<i>d</i>)	Time (RBJD)	Cycle no.	std. dev. (<i>d</i>)	Time (RBJD)	Cycle no.	std. dev. (<i>d</i>)
55019.972986	-1.0	0.000155	55047.622616	9.0	0.000108	55076.647065	19.5	0.000282
55021.350336	-0.5	0.000383	55049.000823	9.5	0.000430	55078.034802	20.0	0.000075
55022.737608	0.0	0.000940	55050.387289	10.0	0.000168	55079.411200	20.5	0.000254
55024.116019	0.5	0.000175	55051.764613	10.5	0.000209	55080.799060	21.0	0.000112
55025.502275	1.0	0.002930	55053.152572	11.0	0.000055	55082.175713	21.5	0.000394
55026.879109	1.5	0.000308	55054.529997	11.5	0.000479	55083.564192	22.0	0.000054
55028.266685	2.0	0.000448	55055.916590	12.0	0.000349	55084.939992	22.5	0.000307
55029.645513	2.5	0.000378	55057.291556	12.5	0.000263	55086.327821	23.0	0.000081
55031.033565	3.0	0.001328	55058.683073	13.0	0.000207	55087.702872	23.5	0.000314
55032.409788	3.5	0.000643	55060.059344	13.5	0.000436	55089.093304	24.0	0.000194
55033.796523	4.0	0.000200	55061.447601	14.0	0.000114	55090.469613	24.5	0.001141
55035.175040	4.5	0.001587	55062.826905	14.5	0.000246	55091.856092	25.0	0.000203
55036.561645	5.0	0.000078	55064.211927	15.0	0.000087	55093.232017	25.5	0.000460
55037.940110	5.5	0.000229	55066.976889	16.0	0.000050	55094.621138	26.0	0.000199
55039.326924	6.0	0.000076	55068.353929	16.5	0.000519	55095.996220	26.5	0.000211
55040.706802	6.5	0.000557	55069.741656	17.0	0.000092	55097.385346	27.0	0.000057
55042.092389	7.0	0.000146	55071.118930	17.5	0.000114	55098.761998	27.5	0.000446
55043.470419	7.5	0.000220	55072.506007	18.0	0.000103	55100.150278	28.0	0.000452
55044.857249	8.0	0.000052	55073.881356	18.5	0.000406	55101.525844	28.5	0.000239
55046.235511	8.5	0.000316	55075.270684	19.0	0.000100	55102.913762	29.0	0.000252

Table A5. Times of minima of CoRoT 110830711

Time (RBJD)	Cycle no.	std. dev. (<i>d</i>)	Time (RBJD)	Cycle no.	std. dev. (<i>d</i>)	Time (RBJD)	Cycle no.	std. dev. (<i>d</i>)
54788.023078	-0.5	0.000402	54824.940971	14.0	0.000050	54863.130202	29.0	0.000059
54789.296425	0.0	0.000236	54826.214821	14.5	0.000241	54864.401442	29.5	0.000133
54790.572760	0.5	0.000168	54827.487298	15.0	0.000056	54866.948855	30.5	0.000479
54791.845541	1.0	0.000065	54828.760033	15.5	0.000118	54869.494468	31.5	0.000117
54793.119517	1.5	0.000180	54830.033262	16.0	0.000068	54870.767700	32.0	0.000065
54794.391327	2.0	0.000079	54832.578973	17.0	0.000075	54872.040394	32.5	0.000283
54795.664033	2.5	0.000199	54833.850810	17.5	0.000126	54873.313283	33.0	0.000079
54796.937032	3.0	0.000056	54835.124576	18.0	0.000065	54874.587249	33.5	0.000160
54798.210657	3.5	0.000306	54836.392527	18.5	0.001064	54875.859268	34.0	0.000051
54799.482707	4.0	0.000068	54837.670751	19.0	0.000077	54877.132981	34.5	0.000129
54800.756760	4.5	0.000121	54838.944440	19.5	0.000209	54878.405360	35.0	0.000081
54802.028493	5.0	0.000062	54840.216662	20.0	0.000072	54879.678157	35.5	0.000122
54803.301066	5.5	0.000254	54841.487854	20.5	0.000294	54880.950873	36.0	0.000070
54804.574266	6.0	0.000080	54842.762557	21.0	0.000088	54882.225031	36.5	0.000240
54805.849405	6.5	0.000282	54844.035997	21.5	0.000109	54883.496662	37.0	0.000078
54807.119961	7.0	0.000058	54845.308887	22.0	0.000063	54884.769767	37.5	0.000187
54808.394553	7.5	0.000218	54846.581572	22.5	0.000236	54886.042394	38.0	0.000063
54809.666055	8.0	0.000058	54847.854569	23.0	0.000088	54887.315450	38.5	0.000149
54810.939690	8.5	0.000253	54849.126682	23.5	0.000128	54888.588111	39.0	0.000062
54812.212004	9.0	0.000073	54850.400722	24.0	0.000066	54889.861642	39.5	0.000257
54813.485392	9.5	0.000177	54851.673887	24.5	0.000159	54891.133899	40.0	0.000076
54814.757655	10.0	0.000051	54852.946496	25.0	0.000069	54892.406984	40.5	0.000223
54816.030821	10.5	0.000239	54854.220417	25.5	0.000252	54893.679800	41.0	0.000089
54817.303532	11.0	0.000055	54855.492376	26.0	0.000093	54894.954592	41.5	0.000256
54818.577371	11.5	0.000150	54856.766127	26.5	0.000085	54896.225738	42.0	0.000074
54819.849472	12.0	0.000072	54858.038690	27.0	0.000074	54897.497495	42.5	0.000157
54821.122230	12.5	0.000291	54859.311530	27.5	0.000093	54898.772165	43.0	0.000082
54822.395180	13.0	0.000067	54860.584306	28.0	0.000069	54900.044392	43.5	0.000184
54823.669011	13.5	0.000101	54861.856686	28.5	0.000163	54901.317483	44.0	0.000081